A Fermionic Portal to Vector Dark Matter from a New Gauge Sector

Alexander Belyaev,[1,*] Aldo Deandrea,[2,†] Stefano Moretti,[1,3,‡] Luca Panizzi,[1,3,§] and Nakorn Thongyoi[1,¶]

[1] *School of Physics and Astronomy, University of Southampton, Highfield, Southampton SO17 1BJ, UK*
[2] *Univ. Lyon, Université Claude Bernard Lyon 1, CNRS/IN2P3, IP2I UMR5822, F-69622, Villeurbanne, France*
[3] *Department of Physics and Astronomy, Uppsala University, Box 516, SE-751 20 Uppsala, Sweden*

We present a class of new physics scenarios wherein the Standard Model (SM) is extended with a new $SU(2)_{\rm D}$ dark gauge sector. These frameworks typically include a $\mathbb{Z}_2$ parity under which states transforming non-trivially under $SU(2)_{\rm D}$ have different parity assignments. After spontaneous breaking of the $SU(2)_{\rm D}$ symmetry via a new scalar doublet, the ensuing massive vector bosons with non-zero D-isospin are Dark Matter (DM) candidates. Non-renormalisable kinetic mixing in the gauge sector or a Higgs portal are not required to connect the dark sector to the SM. We introduce instead a Vector-Like (VL) fermion doublet of $SU(2)_{\rm D}$, the members of which are singlets of the SM Electro-Weak (EW) gauge group, which mediates the interactions between the dark sector and the SM itself. This class of Fermion Portal Vector DM (FPVDM) allows multiple realisations, depending on the properties of the the VL partner and the scalar potential. As a practical example, here, we discuss in detail a realisation involving a VL top partner assuming no mixing between the two scalars of the theory. We then provide bounds from collider and astroparticle observables. The origin of the $\mathbb{Z}_2$ symmetry in this class of models can be justified in the form of a dark EW sector or through an underlying composite structure. The new class of FPVDM models we suggest here has a large number of phenomenological applications depending on the mediator properties and can be used for collider and non-collider studies alike, some of which we outline here for future studies.

* a.belyaev@soton.ac.uk
† deandrea@ipnl.in2p3.fr
‡ s.moretti@soton.ac.uk; stefano.moretti@physics.uu.se
§ luca.panizzi@physics.uu.se
¶ nakorn.thongyoi@gmail.com

CONTENTS

I. INTRODUCTION

The Standard Model (SM) of particle physics describes fundamental particle fields and their interactions under strong, Electro-Magnetic (EM) and weak forces using the symmetry principle of gauge invariance. Further, through the so-called Higgs mechanism, triggering Electro-Weak Symmetry Breaking (EWSB), the last two forces are actually unified into one, the Electro-Weak (EW) one. Given the particle content and charges under the gauge group of the SM, $SU(3)_C \times SU(2)_L \times U(1)_Y$, some of the particles in it are stable either due to the (unbroken) gauge symmetries themselves (like the gluons and photon) or due to the fact that they are the lightest obeying a conservation law (charge or number conservation) such as the electron and its neutrino. The latter is of some importance here, as the analysis of the gravitational interactions at different scales in the Universe carries the prediction of the existence of matter without EM interactions, called Dark Matter (DM), for which a particle interpretation is a natural possibility in the framework of the SM. Herein, the only viable candidate is the aforementioned neutrino, alas, it is not compliant with corresponding experimental observations. Hence, leaving aside other shortcomings of it, there is an obvious need to surpass the SM.

We consider here DM as a vector (spin-1) gauge particle. Such a theoretical construction is extremely well motivated and also constrained in the possible model building choices (see, e.g., [1–24] for discussions of both Abelian and non-Abelian vector DM, in particular using non-renormalisable kinetic mixing terms or Higgs portal scenarios). Our proposal consists in suggesting a set-up where non-Abelian vector DM does not necessarily require non-renormalisable kinetic mixing or a Higgs portal. We propose instead a fermionic portal consisting of, in a minimal construction, a doublet of Vector-Like (VL) fermions under a new "dark" $SU(2)$ group, which are however singlets under the $SU(2)_L$ group. Scenarios with VL portals have also been explored in [25, 26], but for scalar DM candidates. The charge under a new dark gauge group for the DM candidate can induce a phase of dark matter genesis in the early universe (see for example in the $U(1)_D$ case [27]). We do not study this possibility in the following as it goes beyond the minimal model set-up we wish to discuss here. There is also no mandatory reason for a fermionic mediator, but it is an interesting possibility which can be moreover theoretically motivated [28, 29] and is restrictive [30–33]. In the SM the presence of fermions reduces the custodial symmetry of the gauge sector and makes the $W^\pm$ and Z states unstable. In our Fermion Portal Vector Dark Matter (FPVDM) model, the elements of the fermionic doublet have opposite $\mathbb{Z}_2$ parity. This parity is assigned to the different members of $SU(2)_\mathrm{D}$ multiplets and assumed to be different depending on their D-isospin. A discussion of the origin of such a $\mathbb{Z}_2$ parity will be given in the following. A description of the class of models we propose and, in particular, of a minimal set-up is given in the following sections together with a study of the main implications (a selection of such results is presented in Ref. [34]).

The plan of our paper is as follows. The next section describes our model in all its aspects while the following one concentrates on the origin of the $\mathbb{Z}_2$ symmetry. We then look at the phenomenology of a particular realisation of our model, dictated by simplicity and with interesting collider features, wherein we invoke a top-quark portal and eliminate any mixing between SM and dark Higgs bosons.

II. THE DARK SECTOR AND ITS INTERACTIONS WITH THE STANDARD MODEL

We consider an extension of the gauge sector of the SM consisting of a new non-Abelian gauge group for which no renormalisable kinetic mixing terms are allowed. Extra contributions to the kinetic mixing may arise at loop level, depending on the structure of the Higgs sector, but they are suppressed in our case as discussed further in this section. We will consider the $SU(2)$ group, which is the simplest non-Abelian group in terms of number of generators, and in the following it will be labelled as $SU(2)_\mathrm{D}$ since it is associated to the dark sector. The gauge bosons associated to the $SU(2)_\mathrm{D}$ breaking are labelled as $V_\mu^D = \left(V^0_{D+\mu}\ V^0_{D0\mu}\ V^0_{D-\mu}\right)$, where, here and in the following, the superscript identifies the electric charge and the subscript the isospin under $SU(2)_\mathrm{D}$ (D-isospin). The full covariant derivative, including the SM terms, is:

$$D_\mu = \partial_\mu - \left(i\frac{g}{\sqrt{2}}W_\mu^\pm T^\pm + igW_\mu^3 T_3 + ig'YB_\mu\right) - \left(i\frac{g_D}{\sqrt{2}}V^0_{D\pm\mu}T_D^\pm + ig_D V^0_{D0\mu}T_{3D}\right)\ , \tag{2.1}$$

where g and g' are, respectively, the weak and hypercharge coupling constants, g_D is the $SU(2)_\mathrm{D}$ coupling constant, T_3 and Y are the weak-isospin and weak-hypercharge, respectively, while T_{3D} is the dark-isospin associated to $SU(2)_\mathrm{D}$. The indices of the T_D matrices act only on the $SU(2)_\mathrm{D}$ elements and are diagonal with respect to the $SU(2)_L$ ones while the indices of the T matrices act only on the $SU(2)$ elements and are diagonal with respect to $SU(2)_\mathrm{D}$.

Two complex scalar doublets are responsible for the spontaneous breaking of the gauge symmetries of the model:

$$\begin{aligned} \Phi_H &= \begin{pmatrix} \phi^+ \\ \phi^0 \end{pmatrix} \longrightarrow \langle \Phi_H \rangle = \tfrac{1}{\sqrt{2}} \begin{pmatrix} 0 \\ v \end{pmatrix} \quad \text{(scalar doublet breaking } SU(2)_L \times U(1)_Y\text{)} , \\ \Phi_D &= \begin{pmatrix} \varphi^0_{D+1/2} \\ \varphi^0_{D-1/2} \end{pmatrix} \longrightarrow \langle \Phi_D \rangle = \tfrac{1}{\sqrt{2}} \begin{pmatrix} 0 \\ v_D \end{pmatrix} \quad \text{(scalar doublet breaking } SU(2)_{\rm D}\text{)} . \end{aligned} \tag{2.2}$$

A $\mathbb{Z}_2$ parity is introduced to stabilise the actual DM candidate, which is then associated to the lightest $\mathbb{Z}_2$-odd particle of the model. It is now assumed that different members of the same $SU(2)_{\rm D}$ multiplet have a different $\mathbb{Z}_2$ parity. Possible theoretical motivations for this assumption will be developed in section III.

The connection between our dark sector and the SM is achieved by two new VL fermions, which are singlets of $SU(2)_L$ and form a doublet under $SU(2)_{\rm D}$, labelled as $\Psi = (\psi_D,\ \psi)$. This fermion contains a $\mathbb{Z}_2$-odd component and a $\mathbb{Z}_2$-even component which, without loss of generality, can be identified with the $T_{3D} = +1/2$ and $T_{3D} = -1/2$ D-isospin components, respectively (the latter can mix with SM fermions if they share the same quantum numbers). The mass and interaction Lagrangian of the fermion sector is therefore:

$$-\mathcal{L}_f = M_\Psi \bar{\Psi}\Psi + (y \bar{f}^{\rm SM}_L \Phi_H f^{\rm SM}_R + y' \bar{\Psi}_L \Phi_D f^{\rm SM}_R + h.c) , \tag{2.3}$$

where $f^{\rm SM}_{L,R}$ generically denotes a SM left-handed doublet or right-handed singlet, y is the Yukawa coupling of the SM and y' is a new Yukawa coupling connecting the SM fermion with Ψ through the Φ_D doublet. The particle content of the model is summarised in tab. I.

Scalars	$SU(2)_L$	$U(1)_Y$	$SU(2)_{\rm D}$	$\mathbb{Z}_2$
$\Phi_H = \begin{pmatrix} \phi^+ \\ \phi^0 \end{pmatrix}$	**2**	1/2	**1**	+
$\Phi_D = \begin{pmatrix} \varphi^0_{D+\frac{1}{2}} \\ \varphi^0_{D-\frac{1}{2}} \end{pmatrix}$	**1**	0	**2**	$-$ +

Vectors	$SU(2)_L$	$U(1)_Y$	$SU(2)_{\rm D}$	$\mathbb{Z}_2$
$W_\mu = \begin{pmatrix} W^+_\mu \\ W^3_\mu \\ W^-_\mu \end{pmatrix}$	**3**	0	**1**	+ + +
B_μ	**1**	0	**1**	+
$V^D_\mu = \begin{pmatrix} V^0_{D+\mu} \\ V^0_{D0\mu} \\ V^0_{D-\mu} \end{pmatrix}$	**1**	0	**3**	$-$ + $-$

Fermions	$SU(2)_L$	$U(1)_Y$	$SU(2)_{\rm D}$	$\mathbb{Z}_2$
$f^{\rm SM}_L = \begin{pmatrix} f^{\rm SM}_{u,\nu} \\ f^{\rm SM}_{d,\ell} \end{pmatrix}_L$	**2**	$\frac{1}{6}, -\frac{1}{2}$	**1**	+
$u^{\rm SM}_R, \nu^{\rm SM}_R$	**1**	$\frac{2}{3}, 0$	**1**	+
$d^{\rm SM}_R, \ell^{\rm SM}_R$	**1**	$-\frac{1}{3}, -1$	**1**	+
$\Psi = \begin{pmatrix} \psi^D \\ \psi \end{pmatrix}$	**1**	Q	**2**	$-$ +

TABLE I. The quantum numbers under the EW and dark gauge group $SU(2)_{\rm D}$ of the particles of the model. For $SU(2)_L$ and $SU(2)_{\rm D}$, the isospin and dark-isospin representations T and T_D, and their third components T_3 and T_{3D} are provided.

The most general dark Lagrangian is composed of field strength tensors for the vectors (SM and dark), the kinetic and mass terms for the fermions and the scalars, the Yukawa terms and the potential for Φ_H and Φ_D:

$$\begin{aligned} \mathcal{L}_D \supset & -\frac{1}{4}(V^i_{\mu\nu})^2|_{B,W^i,B^0_D,V^0_{Di}} + \bar{f}^{\rm SM} i \not{D} f^{\rm SM} + \bar{\Psi} i \not{D} \Psi + |D_\mu \Phi_H|^2 + |D_\mu \Phi_D|^2 - V(\Phi_H, \Phi_D) \\ & - (y \bar{f}^{\rm SM}_L \Phi_H f^{\rm SM}_R + y' \bar{\Psi}_L \Phi_D f^{\rm SM}_R + h.c) - M_\Psi \bar{\Psi}\Psi . \end{aligned} \tag{2.4}$$

The covariant derivative has been shown in eq. (2.1) and the scalar potential is:

$$V(\Phi_H, \Phi_D) = -\mu^2 \Phi^\dagger_H \Phi_H - \mu^2_D \Phi^\dagger_D \Phi_D + \lambda (\Phi^\dagger_H \Phi_H)^2 + \lambda_D (\Phi^\dagger_D \Phi_D)^2 + \lambda_{\Phi_H \Phi_D} \Phi^\dagger_H \Phi_H \ \Phi^\dagger_D \Phi_D . \tag{2.5}$$

The potential contains a quartic term representing an interaction between the Higgs boson Φ_H and new scalar Φ_D but, as it will be clearer in the following, even for $\lambda_{\Phi_H \Phi_D} = 0$ the fields in the dark sector still interact with the SM through the VL fermion mediator, thus the model does not necessarily require a Higgs portal.

We discuss now in more detail the origin of the kinetic mixing at loop level. The two scalar doublets are secluded with respect to one another in the sense that the SM one has no dark quantum numbers (singlet with respect to $SU(2)_{\rm D}$) and the $SU(2)_{\rm D}$ one has no SM quantum numbers (singlet with respect to the SM). The operator giving rise to kinetic mixing in the effective Lagrangian is a dimension-eight operator, in our case, of the form

$$\frac{1}{\Lambda^4} F^a_{\mu\nu} F_D^{\mu\nu b} \Phi^\dagger_{Hi} (\sigma^a)_{ij} \Phi_{Hj} \Phi^\dagger_{Dk} (\sigma^b)_{kl} \Phi_{Dl} \ , \tag{2.6}$$

where σ^a is a Pauli matrix (generator of $SU(2)_L$) and σ^b is a generator of $SU(2)_{\rm D}$. Here, $F^a_{\mu\nu}$ and $F_D^{\mu\nu b}$ are the field strength tensors of $SU(2)_L$ and $SU(2)_{\rm D}$, respectively. The kinetic mixing term is obtained upon inserting the Vacuum Expectation Values (VEVs) the Higgs doublets but, as already indicated, the operator is suppressed through the fourth power of the large scale Λ. Concerning the origin of this effective operator in our model, the suppression can be estimated with a one-loop two-point function mixing the two types of gauge bosons, $SU(2)_L \times U(1)$ and $SU(2)_{\rm D}$. The fermion loop with four Higgs VEV insertions (two from Φ_H and two from Φ_D) allows to connect the two types of gauge bosons and is expected to be of order:

$$\frac{1}{16\pi^2 M_\Psi^2 m_f^4} y^2 y'^2 g \ g_D v^2 v_D^2 \ , \tag{2.7}$$

where M_Ψ is the mass of the VL fermion Ψ with both weak hypercharge and $SU(2)_{\rm D}$ quantum numbers coupling with a Yukawa type term y' to the Higgs sector.

A gauge mixing term is also possible using the quartic term in the scalar potential $\lambda_{\Phi_H\Phi_D} \Phi^\dagger_H \Phi_H \ \Phi^\dagger_D \Phi_D$, but its contribution is more suppressed as it arises at two loop level.

A. EW and dark symmetry breaking

The minimum of the potential reads as

$$V(\Phi_H, \Phi_D)_{\rm min} = -\frac{\mu^2}{2} v^2 - \frac{\mu_D^2}{2} v_D^2 + \frac{\lambda}{4} v^4 + \frac{\lambda_D}{4} v_D^4 + \frac{\lambda_{\Phi_H\Phi_D}}{4} v^2 v_D^2 \tag{2.8}$$

and the minimization conditions are

$$v(-\mu^2 + \lambda v^2 + \frac{1}{2}\lambda_{\Phi_H\Phi_D} v_D^2) = 0 \quad \text{and} \quad v_D(-\mu_D^2 + \lambda_D v_D^2 + \frac{1}{2}\lambda_{\Phi_H\Phi_D} v^2) = 0 \tag{2.9}$$

while the two non-trivial stationary points are

$$v = \pm\sqrt{\frac{4\lambda_D\mu^2 - 2\lambda_{\Phi_H\Phi_D}\mu_D^2}{4\lambda\lambda_D - \lambda^2_{\Phi_H\Phi_D}}} \quad \text{and} \quad v_D = \pm\sqrt{\frac{4\lambda\mu_D^2 - 2\lambda_{\Phi_H\Phi_D}\mu^2}{4\lambda\lambda_D - \lambda^2_{\Phi_H\Phi_D}}} \ . \tag{2.10}$$

They are minima if the corresponding Hessian matrix is positive definite (i.e., if its eigenvalues are both positive, being a symmetric matrix),

$$\mathcal{H}|_{v_{\rm min}, v_{D\rm min}} = \begin{pmatrix} 3\lambda v^2 - \mu^2 + \frac{\lambda_{\Phi_H\Phi_D}}{2} v_D^2 & \lambda_{\Phi_H\Phi_D} v v_D \\ \lambda_{\Phi_H\Phi_D} v v_D & 3\lambda_D v_D^2 - \mu_D^2 + \frac{\lambda_{\Phi_H\Phi_D}}{2} v^2 \end{pmatrix} \ , \tag{2.11}$$

which, together with the requirements for v and v_D to be real, leads to the following conditions for the Lagrangian parameters:

$$\mu \neq 0 \text{ and } \mu_D \neq 0 \text{ and } \begin{cases} \lambda_{\Phi_H\Phi_D} < 0 \text{ and } \lambda > 0 \text{ and } \lambda_D > 0 \text{ and } \lambda^2_{\Phi_H\Phi_D} < 4\lambda\lambda_D \\ \text{or} \\ \lambda_{\Phi_H\Phi_D} > 0 \text{ and } 2\lambda\mu_D^2 > \lambda_{\Phi_H\Phi_D}\mu^2 \text{ and } 2\lambda_D\mu^2 > \lambda_{\Phi_H\Phi_D}\mu_D^2 \end{cases} . \tag{2.12}$$

Finally, if the Higgs quartic coupling vanishes, $\lambda_{\Phi_H\Phi_D} = 0$, the system simply reduces to two independent potentials, $V(\Phi_H, \Phi_D) = V(\Phi_H) + V(\Phi_D)$, where the two terms have identical structure, corresponding to the SM one, and where the minima are simply defined as:

$$v = \pm\sqrt{\frac{\mu^2}{\lambda}} \quad \text{and} \quad v_D = \pm\sqrt{\frac{\mu_D^2}{\lambda_D}} \ . \tag{2.13}$$

B. Particle spectrum of the model

The model contains new scalar, fermion and vector states. The scalar and fermion ones can mix with SM objects, potentially affecting observables primarily sensitive to the SM itself. In this section, the structure of each particle sector is thus carefully described.

1. Fermions

The fermion component with $T_{3D} = +1/2$ gets only the VL mass, therefore

$$m_{\psi_D} = M_\Psi \ , \tag{2.14}$$

while the other fermion masses are generated after both scalars acquire a VEV. The fermionic mass matrix reads as follow:

$$\mathcal{L}_m^f = (\bar{f}_L^{\rm SM}\psi_L)\mathcal{M}_F \begin{pmatrix} f_R^{\rm SM} \\ \psi_R \end{pmatrix}, \quad \text{with} \quad \mathcal{M}_F = \begin{pmatrix} y\frac{v}{\sqrt{2}} & 0 \\ y'\frac{v_D}{\sqrt{2}} & M_\Psi \end{pmatrix} . \tag{2.15}$$

This mass matrix describes the mixing of a VL fermion with a SM fermion but, unlike in well-known VL scenarios where the new states mix with SM fermions via the Higgs boson, in this case the mixing is driven by Φ_D and the non-zero off-diagonal element is proportional to v_D. The mass matrix can be diagonalised by two unitary matrices, $V_{L,R}$, leading to the mass eigenstates f and F, where f identifies the SM fermion and F its heavier partner:

$$\mathcal{L}_m^f = (\bar{f}_L F_L)\mathcal{M}_F^d \begin{pmatrix} f_R \\ F_R \end{pmatrix} = (\bar{f}_L F_L) V_{fL}^\dagger \mathcal{M}_F V_{fR} \begin{pmatrix} f_R \\ F_R \end{pmatrix} . \tag{2.16}$$

The two rotation matrices $V_{fL} = \begin{pmatrix} \cos\theta_{fL} & \sin\theta_{fL} \\ -\sin\theta_{fL} & \cos\theta_{fL} \end{pmatrix}$ and $V_{fR} = \begin{pmatrix} \cos\theta_{fR} & \sin\theta_{fR} \\ -\sin\theta_{fR} & \cos\theta_{fR} \end{pmatrix}$ diagonalise the products $\mathcal{M}_F^d \mathcal{M}_F^{d\dagger}$ and $\mathcal{M}_F^{d\dagger}\mathcal{M}_F^d$, respectively, and the mass eigenvalues are:

$$m_{f,F}^2 = \frac{1}{4}\left[y^2v^2 + y'^2v_D^2 + 2M_\Psi^2 \mp \sqrt{(y^2v^2 + y'^2v_D^2 + 2M_\Psi^2)^2 - 8y^2v^2M_\Psi^2} \right] . \tag{2.17}$$

The fermion sector contains therefore the SM fermion with mass m_f, a $\mathbb{Z}_2$-even partner with mass m_F and a $\mathbb{Z}_2$-odd partner with mass m_{ψ_D}. The mass hierarchy is $m_f < m_{\psi_D} \leq m_F$.

It is possible to trade the Yukawa parameters for the masses of the physical fermions $\{m_f, m_{\psi_D}, m_F\}$ as:

$$y = \sqrt{2}\frac{m_f m_F}{m_{\psi_D} v}, \quad y' = \sqrt{2}\frac{\sqrt{(m_F^2 - m_{\psi_D}^2)(m_{\psi_D}^2 - m_f^2)}}{m_{\psi_D} v_D} . \tag{2.18}$$

The mixing angles can also be expressed as function of the masses as:

$$\sin^2\theta_{fL} = \frac{m_f^2}{m_{\psi_D}^2}\frac{m_F^2 - m_{\psi_D}^2}{m_F^2 - m_f^2}, \quad \sin^2\theta_{fR} = \frac{m_F^2 - m_{\psi_D}^2}{m_F^2 - m_f^2} . \tag{2.19}$$

The left-handed mixing angle is suppressed by the $m_f^2/m_{\psi_D}^2$ ratio. This feature is different from usual scenarios where a $SU(2)_L$-singlet VL fermion is added to the SM and allowed to mix with SM fermions and where the right-handed mixing angle is suppressed [35]. In this case, despite the fact that ψ is a singlet under the SM gauge group, the mixing is driven by the $SU(2)_{\rm D}$ fermion doublet Ψ and the $SU(2)_{\rm D}$ scalar doublet Φ_D, the elements of which are also singlets under the EW gauge group and hence involves a right-handed SM fermion.

Finally, the new fermion sector is completely decoupled in the limit $m_F = m_{\psi_D}$, for which $y = y_{\rm SM} = \sqrt{2}\frac{m_f}{v}$, $y' = 0$, $\sin\theta_{fL} = \sin\theta_{fR} = 0$, so that the pure SM scenario is restored.

2. $SU(2)_D$ gauge bosons

The kinetic Lagrangian of Φ_H and Φ_D evaluated at the minimum of the scalar potential reads as follows:

$$\mathcal{L}_S^{\rm kin}|_{v,v_D} \supset (\mathcal{V}^0_{\rm SM})^T \mathcal{M}^2_{\mathcal{V}^0_{\rm SM}} \mathcal{V}^0_{\rm SM} + \frac{1}{4} g^2 v^2 W^+ W^- + \frac{1}{8} g_D^2 v_D^2 (V^0_{D0})^2 + \frac{g_D^2}{4} v_D^2 V^0_{D+} V^0_{D-} \ , \tag{2.20}$$

where $\mathcal{V}^0_{{\rm SM}\mu} = (B_\mu \ W^3_\mu)^T$. The SM gauge bosons are not affected by the new Φ_D scalar, and therefore their masses correspond to the SM values. The gauge bosons of $SU(2)_{\rm D}$ are all degenerate and their masses are

$$m_V \equiv m_{V^0_{D\pm}} = m_{V^0_{D0}} = \frac{g_D}{2} v_D \ . \tag{2.21}$$

The only electrically neutral and massive $\mathbb{Z}_2$-odd states of FPVDM scenarios are the $SU(2)_{\rm D}$ gauge bosons $V^0_{D\pm}$, which are thus identified as DM candidates[1]. The degeneracy in mass is broken by the different fermionic loop corrections from f, F and ψ_D corresponding to the different $\mathbb{Z}_2$ parities of the $SU(2)_{\rm D}$ gauge bosons, as shown in fig. 1. For this reason, and for making the notation more compact, we will label the two gauge bosons as:

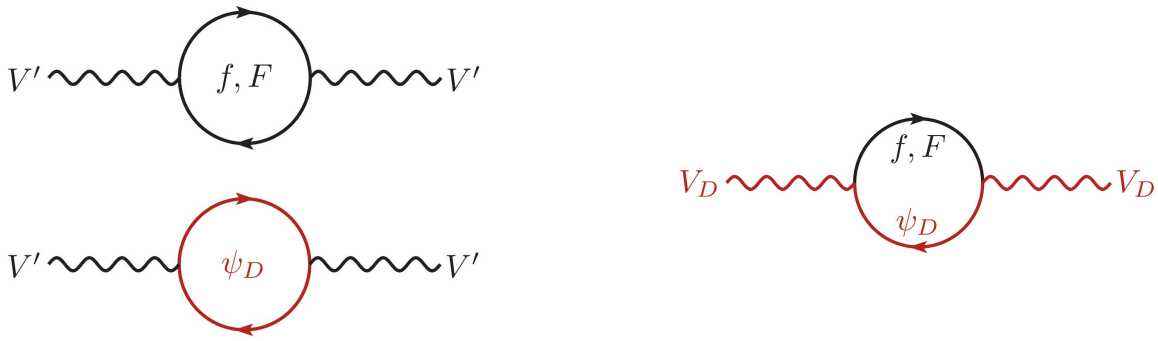

FIG. 1. The Feynman diagrams contributing to mass corrections of $SU(2)_D$ vector bosons, V' (left) and V_D (right) at one loop level. $\mathbb{Z}_2$-odd particles are highlighted in red.

$$\begin{cases} V^0_{D\pm} \equiv V_D & \text{with mass } m_{V_D} \\ V^0_{D0} \equiv V' & \text{with mass } m_{V'} \end{cases} .$$

The detailed discussion of 1-loop calculation is given in appendix A. Here we show that the mass splitting $\Delta m_V = m_{V_D} - m_{V'}$ can be written in a compact form in terms of the parameters

$$\epsilon = \frac{m_F^2 - m_{\psi_D}^2}{m_F^2}, \quad \epsilon_2 = \frac{m_f^2}{m_F^2}, \quad \epsilon_3 = \frac{m_{V_D}^2}{m_F^2} \ , \tag{2.22}$$

in the approximation of $\epsilon, \epsilon_2, \epsilon_3 \ll 1$:

$$\Delta m'_V = \frac{1}{640\pi^2 m_{V_D}} \epsilon g_D^2 m_F^2 \left[(20 + 3\epsilon_3 - 15\epsilon_2 + 20\epsilon_2\epsilon_3) + 10(2\epsilon_2 - \epsilon_3 - 2\epsilon_2\epsilon_3) \log \epsilon_3 \right] + o(\epsilon, \epsilon_2, \epsilon_3) \ . \tag{2.23}$$

For practical purposes, the expression for Δm_V can be further simplified by neglecting ϵ_2 and ϵ_3 and keeping the leading term in ϵ, which leads to the following simple form:

$$\Delta m''_V = \frac{g_D^2 m_F^2}{32\pi^2 m_{V_D}} \epsilon = \frac{g_D^2 m_F^2}{32\pi^2 m_{V_D}} \frac{m_F^2 - m_{\psi_D}^2}{m_F^2} . \tag{2.24}$$

The radiative mass splitting between the V_D and V' bosons plays a very important role in the determination of relic density and DM Indirect Detection (ID) rates. The range of validity of the approximations for Δm_V presented above depends on the specific realisation of the FPVDM model and the model parameter space. A detailed discussion of the respective numerical results for Δm_V is given in section IV for a specific case study.

[1] In principle, the introduction of VL neutrino partners could make the $\mathbb{Z}_2$-odd member of the VL doublet a DM candidate, but a mixing in the neutrino sector would require further new physics to account for neutrino mass generation. This non-minimal scenario is not considered in the present analysis though.

3. Scalars

The scalar potential of eq. (2.5) is constructed starting from the 8 degrees of freedom of all the scalar fields of the theory: 4 for Φ_H and 4 for Φ_D. The theory contains 6 massive gauge bosons: Z, $W^\pm$, V' and V_D (with two opposite D-isospin values). Therefore 6 Goldstone bosons are needed to give the corresponding longitudinal components. Two degrees of freedom are left, which correspond to physical massive scalars: the SM Higgs boson, h, and a further CP-even scalar, H. By denoting the neutral scalars in the interaction eigenstates in terms of their components in the unitary gauge as

$$\phi^0 = \frac{1}{\sqrt{2}}(v + h_1) \,, \tag{2.25}$$

$$\varphi^0_{D-1/2} = \frac{1}{\sqrt{2}}(v_D + \varphi_1) \,, \tag{2.26}$$

the Lagrangian terms for scalar masses can be written as:

$$\mathcal{L}^{\mathcal{S}}_m = (h_1 \; \varphi_1) \begin{pmatrix} \lambda v^2 & \frac{\lambda_{\Phi_H \Phi_D}}{2} v v_D \\ \frac{\lambda_{\Phi_H \Phi_D}}{2} v v_D & \lambda_D v_D^2 \end{pmatrix} \begin{pmatrix} h_1 \\ \varphi_1 \end{pmatrix} \,. \tag{2.27}$$

The mass eigenvalues can be obtained by diagonalising the mass matrix via a rotation matrix $V_S = \begin{pmatrix} \cos\theta_S & \sin\theta_S \\ -\sin\theta_S & \cos\theta_S \end{pmatrix}$ and are

$$m^2_{h,H} = \lambda v^2 + \lambda_D v_D^2 \mp \sqrt{(\lambda v^2 - \lambda_D v_D^2)^2 + \lambda^2_{\Phi_H \Phi_D} v^2 v_D^2} \tag{2.28}$$

while the mixing angle is

$$\sin\theta_S = \sqrt{2 \frac{m_H^2 v^2 \lambda - m_h^2 v_D^2 \lambda_D}{m_H^4 - m_h^4}} \,. \tag{2.29}$$

Even in the absence of explicit mixing induced by the quadratic term, i.e. even if $\lambda_{\Phi_H \Phi_D} = 0$, h_1 and φ_1 can mix at one-loop via the their interactions with fermions. The consequences of this mixing, which can also affect Higgs-related observables, go beyond the scopes of this analysis, and will be treated in a future work.

C. Flavour structure and Cabibbo-Kobayashi-Maskawa (CKM) matrix

The previous treatment assumed the presence of one VL $SU(2)_{\rm D}$ doublet interacting with one SM fermion, without specifying the flavour structure involved. If the full flavour structure of the SM is considered, different possibilities might arise. A VL fermion can interact with one or more SM flavours and there can be multiple VL fermions.

The most general Lagrangian, representing the previous possibilities, is

$$\begin{aligned} \mathcal{L}_m = & M_U^I \bar{U}_I U_I + M_D^J \bar{D}_J D_J + M_E^K \bar{E}_K E_K \\ & + y_u^i \bar{Q}^{\rm SM}_{iL} \tilde{\Phi}_H u^{\rm SM}_{iR} + y_d^i \tilde{V}^{ij}_{\rm CKM} \bar{Q}^{\rm SM}_{iL} \Phi_H d^{\rm SM}_{jR} + y_l^i \bar{L}^{\rm SM}_{iL} \Phi_H l^{\rm SM}_{iR} + h.c. \\ & + (y'_u)^{Ij} \bar{U}_{IL} \Phi_D u^{\rm SM}_{jR} + (y'_d)^{Jj} \bar{D}_{JL} \Phi_D d^{\rm SM}_{jR} + (y'_l)^{Kj} \bar{E}_{KL} \Phi_D l^{\rm SM}_{jR} + h.c. \,, \end{aligned} \tag{2.30}$$

where $\tilde{\Phi}_H = i\tau_2 \Phi_H^*$, $i, j = 1, 2, 3$ are SM flavour indices and I, J, K run over the flavours of the VL partners. The SM Yukawas have been diagonalised exploiting the flavour symmetries and the SM CKM matrix (i.e. the CKM matrix if no VL states were introduced) and $\tilde{V}_{\rm CKM}$ has been introduced to parametrise the misalignment between the flavour and mass eigenstates in the down sector.

The most generic mass matrices read as follows:

$$\mathcal{M}_U = \left(\begin{array}{c|c} y_u^i \frac{v}{\sqrt{2}} & 0^{iI} \\ \hline (y'_u)^{Ii} \frac{v_D}{\sqrt{2}} & M_U^I \end{array} \right) \,, \quad \mathcal{M}_D = \left(\begin{array}{c|c} y_d^i \tilde{V}^{ij}_{\rm CKM} \frac{v}{\sqrt{2}} & 0^{iJ} \\ \hline (y'_d)^{Ji} \frac{v_D}{\sqrt{2}} & M_D^J \end{array} \right) \,, \quad \mathcal{M}_E = \left(\begin{array}{c|c} y_l^i \frac{v}{\sqrt{2}} & 0^{iK} \\ \hline (y'_l)^{Ki} \frac{v_D}{\sqrt{2}} & M_E^K \end{array} \right) \,. \tag{2.31}$$

The mass matrices can be diagonalised by two unitary matrices V_L and V_R, with dimension $3 + \{I, J, K\}$ depending on the fermion type. If the same VL fermion interacts with multiple flavours of SM fermions, the most constraining

effects are represented by modifications to SM observables, induced by Flavour Changing Neutral Currents (FCNCs) [36, 37]. If for each SM fermion there is a VL partner, the matrix proportional to y' is diagonal as well and no mixing is induced between different SM and VL flavours, thus fermions from the dark sector only interact with the corresponding SM flavour. In the following we will limit the analysis to this simpler scenario.

An important property of this construction is that the CKM matrix of the SM receives contributions from new physics. In fact, the SM charged current is

$$\begin{aligned} J^\mu_{W^+} &= \frac{g}{\sqrt{2}}(\bar{u}_L^{\text{SM i}}\ \bar{U}_L^I)\gamma^\mu \left(\begin{array}{c|c} 1_{3\times3} & 0^{3J} \\ \hline 0^{I3} & 0^{IJ} \end{array}\right) \begin{pmatrix} d_L^{\text{SM i}} \\ D_L^J \end{pmatrix} \\ &= \frac{g}{\sqrt{2}}(\bar{u}_L^i\ \bar{u}_L'^I)\gamma^\mu V_{uL}^\dagger \left(\begin{array}{c|c} \tilde{V}_{\text{CKM}} & 0^{3J} \\ \hline 0^{I3} & 0^{IJ} \end{array}\right) V_{dL} \begin{pmatrix} d_L^i \\ d_L'^J \end{pmatrix} , \end{aligned} \tag{2.32}$$

such that the entries of the measured CKM matrix are given by

$$V_{CKM}^{ij} = (V_{uL}^\dagger)^{ik}\tilde{V}_{\text{CKM}}^{kl}V_{dL}^{kj} . \tag{2.33}$$

D. FPVDM parameter space

The Lagrangian parameters of the model are the following:

- gauge couplings: g, g', g_D;
- Scalar potential parameters: $\mu, \lambda, \mu_D, \lambda_D, \lambda_{\Phi_H\Phi_D}$;
- Yukawa couplings and VL quark mass: y, y', m_{ψ_D};
- $\tilde{V}_{\text{CKM}}$ parameters.

Assuming that the new VL fermion interacts only with one SM flavour, these parameters can be traded for the masses of all the physical states, the weak coupling constant g (or equivalently, the fine structure constant α_{EM}), the new gauge coupling g_D, the mixing angle between the scalar fields θ_S and the measured CKM parameters. A complete set of parameters is therefore:

$$\{g, m_W, m_Z\},\ \{g_D, m_{V_D}\},\ \{m_h, m_H, \sin\theta_S\},\ \{m_f, m_F, m_{\psi_D}\} \text{ and } V_{\text{CKM}} , \tag{2.34}$$

but, since g, m_W, m_Z, m_h, m_f and V_{CKM} are precisely measured SM parameters, we are left with the following six independent new physics parameters, namely:

$$g_D, m_{V_D}, m_H, \sin\theta_S, m_F, m_{\psi_D} . \tag{2.35}$$

Approximating the CKM as a diagonal matrix for simplicity, the relations between the Lagrangian parameters connected to the new physics components and the input parameters take a very simple form:

$$v = \frac{2m_W}{g}, \quad v_D = \frac{2m_{V_D}}{g_D} , \tag{2.36}$$

$$\lambda = \frac{g^2}{8m_W^2}(m_h^2\cos^2\theta_S + m_H^2\sin^2\theta_S) , \tag{2.37}$$

$$\lambda_D = \frac{g_D^2}{8m_{V_D}^2}(m_h^2\sin^2\theta_S + m_H^2\cos^2\theta_S) , \tag{2.38}$$

$$\lambda_{\Phi_H\Phi_D} = \frac{g\ g_D}{8m_W m_{V_D}}(m_H^2 - m_h^2)\sin 2\theta_S , \tag{2.39}$$

$$\mu^2 = \frac{1}{2}\left(m_h^2\cos^2\theta_S + m_H^2\sin^2\theta_S + \frac{1}{2}\frac{g}{g_D}\frac{m_{V_D}}{m_W}(m_H^2 - m_h^2)\sin 2\theta_S\right) , \tag{2.40}$$

$$\mu_D^2 = \frac{1}{2}\left(m_h^2\sin^2\theta_S + m_H^2\cos^2\theta_S + \frac{1}{2}\frac{g_D}{g}\frac{m_W}{m_{V_D}}(m_H^2 - m_h^2)\sin 2\theta_S\right) , \tag{2.41}$$

$$y = \frac{g\ m_f\ m_F}{\sqrt{2}m_{\psi_D}m_W} , \tag{2.42}$$

$$y' = \frac{g_D\sqrt{(m_F^2 - m_{\psi_D}^2)(m_{\psi_D}^2 - m_f^2)}}{\sqrt{2}m_{\psi_D}m_{V_D}} . \tag{2.43}$$

The minimisation conditions of the scalar potential in eq. (2.12) are automatically satisfied. If $\lambda_{\Phi_H\Phi_D} < 0$, which corresponds to $m_h > m_H$, the condition $\lambda^2_{\Phi_H\Phi_D} < 4\lambda\lambda_D$ translates into $\frac{1}{16}\frac{g^2 g_D^2}{m_W^2 m_{V_D}^2} m_h^2 m_H^2 > 0$, which is always true, while, if $\lambda_{\Phi_H\Phi_D} > 0$, the conditions $2\lambda\mu_D^2 > \lambda_{\Phi_H\Phi_D}\mu^2$ and $2\lambda_D\mu^2 > \lambda_{\Phi_H\Phi_D}\mu_D^2$ translate into $\frac{1}{8}\frac{g^2}{m_W^2} m_h^2 m_H^2 > 0$ and $\frac{1}{8}\frac{g_D^2}{m_{V_D}^2} m_h^2 m_H^2 > 0$, respectively, again automatically satisfied.

For a perturbative analysis of the parameter space we need to identify the regions where coupling parameters do not become too large, in order to make sure that all predictions on the model are reliable. A complete loop description of all the sectors of the model is beyond the scope of this analysis and therefore we assume that perturbativity is achieved by the requirement for all couplings of the FPVDM model to be (optimistically) below 4π. For example, the requirement $\lambda < 4\pi$ defines the maximal value of m_H for a given value of the scalar mixing angle, θ_S, as shown by the blue contour in the left panel of fig. 2. The same figure presents contours for the g_D/m_{V_D} ratio in the $\{m_H, \theta_S\}$ plane corresponding to $\lambda_D = 4\pi$, which indicates the perturbativity limit on the respective parameters.

The perturbative constraints on the Yukawa couplings y and y' imply that the ratio between the masses of the new fermions F and ψ_D cannot be too large. The condition for y reads as $\frac{m_F}{m_{\psi_D}} < 4\pi\frac{\sqrt{2}m_W}{g m_f}$. At the same time, the $y' < 4\pi$ condition is defined also by the g_D/m_{V_D} ratio, as one can see from eq. (2.43). Both constraints from y and y' perturbativity requirements are presented in the right panel of fig. 2 in the $(m_{\psi_D}, \frac{m_F}{m_{\psi_D}})$ plane. In our analysis of the parameter space we indicate the respective regions where perturbativity constraints are violated.

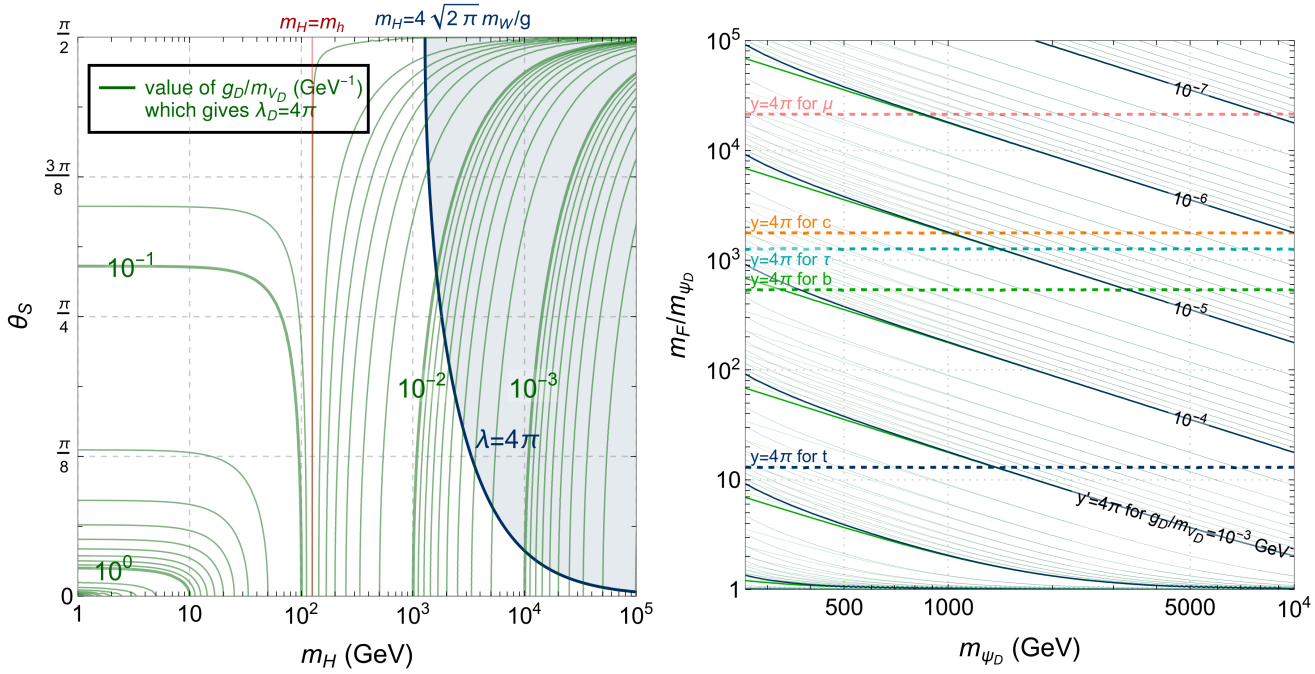

FIG. 2. Left: the maximum value of m_H and minimum value of θ_S for $\lambda < 4\pi$ and $\lambda_D < 4\pi$ as function of $\frac{g_D}{m_{V_D}}$. The regions corresponding to $\lambda_D < 4\pi$ are to the left of the green lines. Right: the maximum value of the m_F/m_{ψ_D} ratio as function of m_{ψ_D} and $\frac{g_D}{m_{V_D}}$, and under different hypotheses about which SM fermion interacts with the $SU(2)_{\rm D}$ doublet Ψ, to satisfy the perturbativity conditions $\{y, y'\} < 4\pi$.

III. ON THE ORIGIN OF THE $\mathbb{Z}_2$ PARITY

One of the main open questions of the construction presented in this analysis is the origin of the $\mathbb{Z}_2$ parity. In section II this parity has been *assigned* to the different members of $SU(2)_{\rm D}$ multiplets and assumed to be different depending on their D-isospin. However, a theoretical origin of the parity would provide a robust ground for the consistency of the model. In this section we explore two options for explaining the origin of the $\mathbb{Z}_2$ parity.

The first involves the existence of a further $U(1)_{\rm D}$ extension of the gauge group in the dark sector, which would generate a mirror version of the SM EW sector, the two of which can be connected by the mixed $(\Phi^\dagger\Phi)(\Phi_D^\dagger\Phi_D)$

quartic term in the full potential and by the gauge kinetic mixing between $U(1)_Y$ and $U(1)_D$. In this scenario the $\mathbb{Z}_2$ parity would be associated to a dark-charge all in all analogous to the EM charge of QED, thus giving literal meaning to the notation V^0_{D0} and $V^0_{D\pm}$ for the $SU(2)_{\rm D}$ gauge bosons in the dark sector.

The second involves the existence of a strongly-coupled sector whose condensates form the particle in the low energy regime, in particular, a residual parity for the composite sector is present due to the specific vacuum alignment present in this kind of models (which would typically also imply an extended Higgs sector). A detailed discussion is given in [38] and further used in [39] for the case of a scalar DM candidate.

A. A dark EW sector

In this scenario the SM is augmented with a dark sector constructed starting from a dark gauge group $\mathcal{G}_D$ with same structure as the EW gauge group of the SM. The gauge group is spontaneously broken as:

$$\mathcal{G} = \mathcal{G}_{\rm SM} \times \mathcal{G}_D = SU(2)_L \times U(1)_Y \times SU(2)_{\rm D} \times U(1)_{\rm YD} \longrightarrow U(1)_{\rm EM} \times U(1)_{\rm D} \ . \tag{3.1}$$

The gauge boson associated to $U(1)_{\rm YD}$ is labelled as $B^0_{D0\mu}$. The full covariant derivative is:

$$D_\mu = \partial_\mu - \left(i\frac{g}{\sqrt{2}} W^\pm_\mu T^\pm + igW^3_\mu T_3 + ig' Y B_\mu \right) - \left(i\frac{g_D}{\sqrt{2}} V^0_{D\pm\mu} T^\pm_D + ig_D V^0_{D0\mu} T_{3D} + ig'_D Y_D B^0_{D0\mu} \right) \ , \tag{3.2}$$

where g and g' are, respectively, the weak and hypercharge coupling constants, g_D and g'_D are the $SU(2)_{\rm D}$ and $U(1)_{\rm YD}$ coupling constants, T_3 and Y are the weak-isospin and weak-hypercharge, T_{3D} and Y_D are the dark-isospin associated to $SU(2)_{\rm D}$ and the dark-hypercharge associated to $U(1)_{\rm YD}$ and where the indices of the T_D matrices act only on the $SU(2)_{\rm D}$ elements and are diagonal with respect $SU(2)_L$ while the indices of the T matrices act only on the $SU(2)$ elements and are diagonal with respect to $SU(2)_{\rm D}$.

The unbroken $U(1)_{\rm D}$ continuous symmetry is associated to a conserved charge, labelled D-charge, defined as:

$$Q_D = T_{3D} + Y_D \ . \tag{3.3}$$

Notice that *the D-charge is not associated with the electric charge*: electrically neutral particles can be D-charged and vice versa. The only assumption to be made in this scenario is that *all the SM states are neutral under the conserved D-charge* Q_D. This however does not necessarily imply that all the states of new physics are charged under $U(1)_{\rm D}$ or that they must be neutral under the conserved SM charges.

The fields responsible for the breaking of the gauge symmetry are the two scalar doublets Φ_H and Φ_D described in section II. Since Φ_H is singlet with respect to the dark gauge group and Φ_D is singlet with respect to the EW gauge group, given the absence of gauge kinetic mixing terms, no mixing is induced between the fully neutral gauge bosons W^3_μ, B_μ, $V^0_{D0\mu}$ and $B^0_{D0\mu}$, In complete analogy with the SM, by counting the number of bosonic degrees of freedom, one massless gauge boson is predicted in the dark gauge sector and the other dark gauge bosons receive different masses. We can thus define the mass eigenstates γ_D, Z^0_D and $W^0_{D\pm}$ with values

$$M_{\gamma_D} = 0 \ , \tag{3.4}$$

$$M_{Z^0_D} = \frac{1}{2}\sqrt{g_D^2 + g_D'^2}\ v_D \ , \tag{3.5}$$

$$M_{W^0_{D\pm}} = \frac{g_D}{2} v_D \ , \tag{3.6}$$

such that the masses of the DM vector $V^0_{D\pm}$ and of the D-charge-neutral gauge boson V^0_{D0} receive a splitting proportional to $\frac{1}{2}g'_D v_D$. The particle content of the model is summarised in tab. II.

The presence of two $U(1)$ gauge groups, however, allows for the existence of a renormalisable and gauge-invariant kinetic mixing term, such that the Lagrangian of the $U(1)_Y \times U(1)_{\rm YD}$ sector is:

$$-\mathcal{L}_{\rm KM} = \frac{1}{4} B_{\mu\nu} B^{\mu\nu} + \frac{1}{4} B_{D\mu\nu} B^{\mu\nu}_D + \frac{\varepsilon}{2} B_{\mu\nu} B^{\mu\nu}_D \ , \tag{3.7}$$

where $B_{D\mu\nu}$ is the field tensor of $U(1)_{\rm YD}$ and ε is the kinetic mixing parameter. The diagonalisation of the kinetic terms can be obtained through the rotation [40]:

$$\begin{pmatrix} B^\mu \\ B^{0\mu}_{D0} \end{pmatrix} = \begin{pmatrix} \frac{1}{\sqrt{1-\varepsilon^2}} & 0 \\ -\frac{\varepsilon}{\sqrt{1-\varepsilon^2}} & 1 \end{pmatrix} \begin{pmatrix} \cos\theta_k & -\sin\theta_k \\ \sin\theta_k & \cos\theta_k \end{pmatrix} \begin{pmatrix} B^\mu_1 \\ B^\mu_2 \end{pmatrix} \tag{3.8}$$

	EW		Dark		Unbroken	
	$SU(2)_L$	$U(1)_Y$	$SU(2)_\mathrm{D}$	$U(1)_\mathrm{YD}$	$U(1)_\mathrm{EM}$	$U(1)_\mathrm{D}$
Scalar fields						
$\Phi_H = \begin{pmatrix}\phi^+\\ \phi^0\end{pmatrix}$	$\mathbf{2}$	$1/2$	$\mathbf{1}$	0	$\begin{matrix}1\\0\end{matrix}$	$\begin{matrix}0\\0\end{matrix}$
$\Phi_D = \begin{pmatrix}\varphi^0_{D+\frac{1}{2}}\\ \varphi^0_{D-\frac{1}{2}}\end{pmatrix}$	$\mathbf{1}$	0	$\mathbf{2}$	$1/2$	$\begin{matrix}0\\0\end{matrix}$	$\begin{matrix}1\\0\end{matrix}$
Fermion fields						
$f^\mathrm{SM}_L = \begin{pmatrix}f^\mathrm{SM}_{u,\nu}\\ f^\mathrm{SM}_{d,\ell}\end{pmatrix}_L$	$\mathbf{2}$	$1/6, -1/2$	$\mathbf{1}$	0	$T_{3f}+Y_f$	0
$u^\mathrm{SM}_R, \nu^\mathrm{SM}_R$	$\mathbf{1}$	$2/3, 0$	$\mathbf{1}$	0	$T_{3f}+Y_f$	0
$d^\mathrm{SM}_R, \ell^\mathrm{SM}_R$	$\mathbf{1}$	$-1/3, -1$	$\mathbf{1}$	0	$T_{3f}+Y_f$	0
$\Psi = \begin{pmatrix}\psi^D\\ \psi\end{pmatrix}$	$\mathbf{1}$	Q_Ψ	$\mathbf{2}$	$1/2$	Q_Ψ	$\begin{matrix}1\\0\end{matrix}$
Vector fields						
$W_\mu = \begin{pmatrix}W^+_\mu\\ W^3_\mu\\ W^-_\mu\end{pmatrix}$	$\mathbf{3}$	0	$\mathbf{1}$	0	$\begin{matrix}1\\0\\-1\end{matrix}$	$\begin{matrix}0\\0\\0\end{matrix}$
B_μ	$\mathbf{1}$	0	$\mathbf{1}$	0	0	0
$V_{D\mu} = \begin{pmatrix}V^0_{D+\mu}\\ V^0_{D0\mu}\\ V^0_{D-\mu}\end{pmatrix}$	$\mathbf{1}$	0	$\mathbf{3}$	0	$\begin{matrix}0\\0\\0\end{matrix}$	$\begin{matrix}1\\0\\-1\end{matrix}$
$B^0_{D0\mu}$	$\mathbf{1}$	0	$\mathbf{1}$	0	0	0

TABLE II. The quantum numbers under the EW and dark gauge group $SU(2)_\mathrm{D} \times U(1)_\mathrm{D}$ of the particles of the model. The charges of the unbroken groups $U(1)_\mathrm{EM}$ and $U(1)_\mathrm{D}$ are also provided.

The kinetic-mixing term induces a modification in the mass mixing matrix of the fully neutral gauge bosons. Upon diagonalisation, two massless eigenstates are obtained, corresponding to the SM photon and to a massless dark photon, and two massive eigenstates, corresponding to the Z boson and to a massive Z' boson. The full expressions of the mass mixing matrix and of the mass eigenstates can be found in appendix B. Expanding the mass eigenstates of Z and Z' for small ε, the lowest order terms assume a simple form:

$$M_Z^2 = \frac{v^2}{4}\left[g^2 + g'^2\left(1 + \frac{(g^2+g'^2)v^2 - g_D^2 v_D^2}{(g^2+g'^2)v^2 - (g_D^2+g_D'^2)v_D^2}\varepsilon^2\right)\right] + \mathcal{O}(\varepsilon^4)\,, \tag{3.9}$$

$$M_{Z'}^2 = \frac{v_D^2}{4}\left[g_D^2 + g_D'^2\left(1 + \frac{g^2 v^2 - (g_D^2+g_D'^2)v_D^2}{(g^2+g'^2)v^2 - (g_D^2+g_D'^2)v_D^2}\varepsilon^2\right)\right] + \mathcal{O}(\varepsilon^4)\,, \tag{3.10}$$

which in the $\varepsilon \to 0$ limit (no kinetic mixing) reduce to the SM value and eq.(3.5), respectively. The implications of this scenario and the derivation of its experimental bounds are beyond the scope of this analysis and are reserved for future developments.

B. A composite origin

In the case of composite models the discrete symmetries allowing the stability of the DM particle depend on the model building details of the composite sector. However, this does not mean that the DM candidate and the corresponding discrete symmetries are an arbitrary choice. The composite effective chiral Lagrangian is invariant under a parity changing the signs of all the pseudo Nambu-Goldstone Bosons (pNGBs), as they appear in bilinear

terms in the Lagrangian. Furthermore, these models contain by construction explicit symmetry breaking terms, so more scrutiny is needed to understand if a pNGB can be stable due to a residual parity and therefore be used as a particle describing DM. The origin of the non-invariance with respect to parity (and also charge conjugation) is due to the choice of the vacuum while the strong techni-sector at the origin of these models is instead parity invariant as it is VL with respect to the composite gauge dynamics and the SM gauge group. Once possible parities acting on the pNGBs are identified, these models require a careful check of their invariance, including the Wess-Zumino-Witten terms. In explicit realisations studied in the literature, e.g., in [38, 39], a stable pNGB multiplet allowing the description of DM can indeed be found.

IV. A CASE STUDY: TOP PORTAL WITH NO MIXING BETWEEN h AND H

This section is dedicated to a specific realisation of the model. It is assumed that only one VL partner exists, and interacts exclusively with the SM top quark, plus it is further assumed that the Higgs bosons h and H do not mix, i.e., $\theta_S = 0$. These choices significantly simplify the expressions of the Lagrangian parameters, which read:

$$v = \frac{2m_W}{g},\ \mu^2 = \frac{m_h^2}{2},\ \lambda = \frac{g^2 m_h^2}{8m_W^2}, \tag{4.1}$$

$$v_D = \frac{2m_{V_D}}{g_D},\ \mu_D^2 = \frac{m_H^2}{2},\ \lambda_D = \frac{g_D^2 m_H^2}{8m_{V_D}^2},\ \lambda_{\Phi_H \Phi_D} = 0, \tag{4.2}$$

$$y_t = \frac{g\, m_t\, m_T}{\sqrt{2} m_{t_D} m_W} = y_t^{\rm SM} \frac{m_T}{m_{t_D}}, \quad y_t' = \frac{g_D \sqrt{(m_T^2 - m_{t_D}^2)(m_{t_D}^2 - m_t^2)}}{\sqrt{2} m_{t_D} m_{V_D}}\ , \tag{4.3}$$

where the $\mathbb{Z}_2$-even(-odd) partner of the top quark has been labelled $T(t_D)$, the SM Higgs sector is left unaffected by the new scalar, and Φ_D has a potential completely analogous to the Higgs one. The hierarchy between the masses in the fermion sector is the same as discussed in section II B 1, i.e. $m_t < m_{t_D} \leq m_T$, but H can have any mass allowed by experimental bounds, including being lighter than the SM Higgs boson in principle.

The respective new physics parameter space for this model is five-dimensional:

$$g_D, m_{V_D}, m_H, m_T, m_{t_D}\ . \tag{4.4}$$

We chose this realisation as a case study since, on the one hand, it is minimal while, on the other hand, it allows to explore a scenario where a non-Abelian dark sector is not connected to the SM via a Higgs portal at tree level. Furthermore, connecting the dark sector only with the SM top quark allows for an exploration of multiple interesting signatures at collider while reducing the impact of constraints from direct detection.

As anticipated in section II B 2, the mass splitting between m_{V_D} and $m_{V'}$, $\Delta m_V = m_{V_D} - m_{V'}$, plays an important role for DM phenomenology. First of all, we have that $\Delta m_V > 0$ in the whole parameter space of the model, with the approximate expressions for Δm_V given by eqs. (2.23) and (2.24). Since $m_{V_D} > m_{V'}$, $V_D V_D^* \to V'V'$ process for DM annihilation will *always* take place for any point in the parameter space to crucially contribute to the list of processes defining relic density and to extend the viable parameter space from the relic density constraints point of view. The $V_D V_D^* \to V'V'$ process will also contribute to the DM indirect detection signal.

Numerically, the value of Δm_V varies in a very wide range, as it scales as g_D^2 and it is proportional to $m_T^2 - m_{t_D}^2$. One should also note that Δm_V does not depend on m_H. In fig. 3 (left) we present the iso-contours for Δm_V in the $\{m_{t_D}, m_{V_D}\}$ plane for $g_D = 0.1$ and $m_T = 1600$ GeV, while in fig. 3 (right) we show how Δm_V evolves as function of m_{V_D} for the specific value of $m_{t_D} = 1590$ GeV, all other parameters being the same. The value of m_T is chosen to be safely above the current upper limit on VL top partners at the LHC [41]. For our particular choice of g_D and m_T, Δm_V can be as large as 1 GeV, while its minimal value reaches zero for a vanishing value of $m_T - m_{t_D}$. In both frames we present a comparison of the exact one-loop result for Δm_V and its approximations given by eqs. (2.23) and (2.24). It is possible to see from fig. 3 (right) that the approximate formulae are very accurate for a small $m_T - m_{t_D}$ splitting, but break down for m_{V_D} close to the $m_t + m_{\psi_D}$ threshold, where the one-loop corrections are highly non-linear with respect to the expansion parameters used in approximate expressions for Δm_V. Moreover, for small values of m_{V_D}, the one-loop mass corrections can be large, making the evaluation of Δm_V unstable perturbatively. Therefore, we indicate the region where one-loop corrections to the masses of V_D and/or V' become larger than 50% by the hatched area.

The lifetime of V' does not directly depend on Δm_V. However, the $\mathbb{Z}_2$-even $SU(2)_{\rm D}$ gauge boson can also be long lived, if the DM is light enough. The only tree-level interaction of V' with SM particles is with top quarks, due to its mixing with T. If the mass of V' drops below the $t\bar{t}$ threshold, it can only decay directly to a three-body or four-body

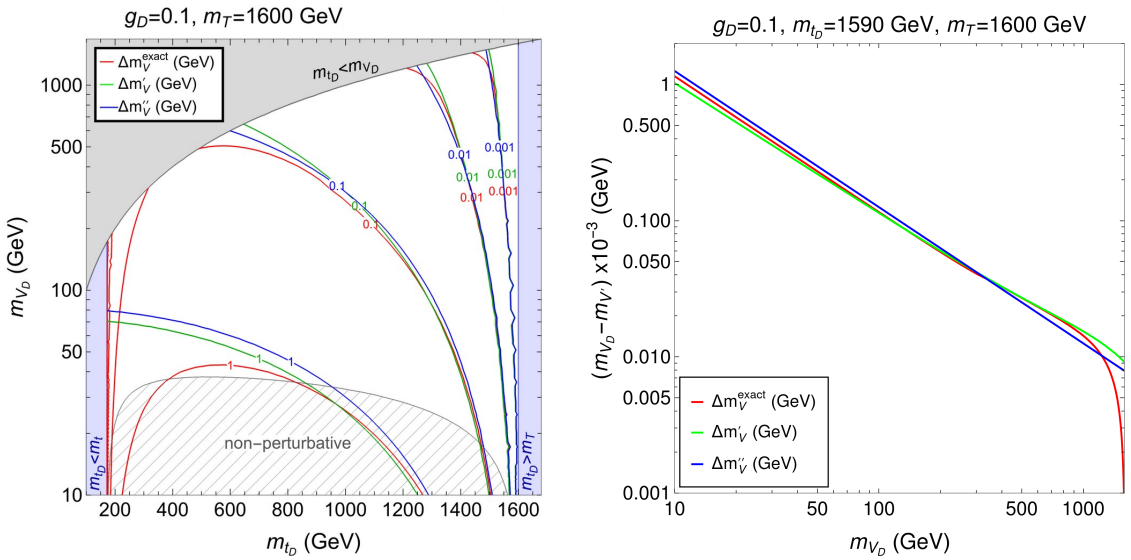

FIG. 3. Values of the mass splitting $\Delta m_V = m_{V_D} - m_{V'}$ in the (m_{t_D}, m_{V_D}) plane for a specific choice of g_D, m_T and m_H(left panel) and as a function of m_{V_D} for a specific value of m_{t_D} (right panel). The red, green and blue curves correspond to results from exact expression, approximated formulae eq. (2.23) and eq. (2.24), respectively. The region where one-loop corrections to the masses of V_D or V' become larger than 50%, so that a perturbative treatment is questionable, is also highlighted.

final state with W bosons and b quarks via the off-shell top quarks, or decay to a $b\bar{b}$ final state at one-loop, see the Feynman diagrams fig. 4(left). The latter, although suppressed by the loop factor, becomes dominant due to the smaller phase space, as shown in fig. 4(centre and right). This loop-induced diagrams prevent V' to live too long to spoil Big Bang Nucleo-synthesis (BBN) but, when the g_D coupling is small, the t_D mass approaches the decoupling limit ($m_{t_D} = m_T$) and the DM is light, so V' becomes long lived at colliders. Therefore, it could provide a signal for searches of long-lived neutral bosons decaying into $b\bar{b}$ pairs.

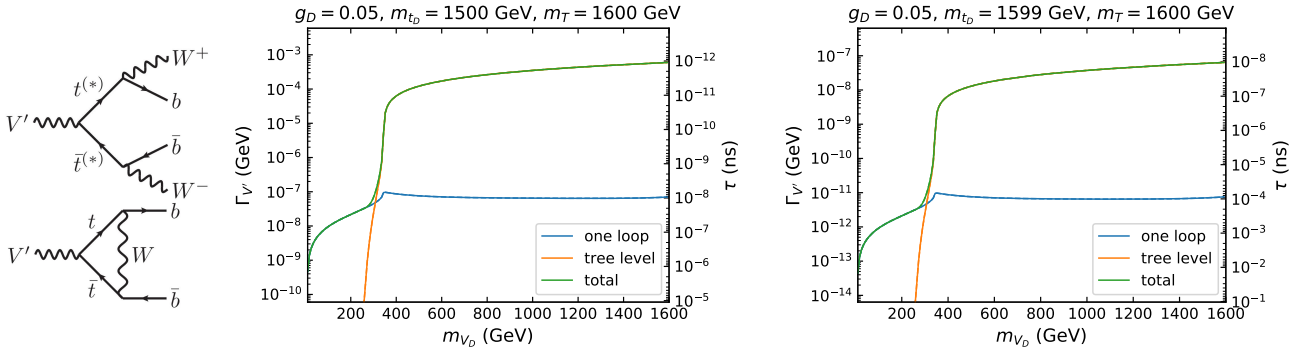

FIG. 4. Left: Tree-level and one-loop diagrams for V' decay. Center and right: decay width and lifetime of V' at tree and one-loop level for $g_D = 0.05$, $m_T = 1600$ GeV and different values of m_{t_D}.

In the following sections, this model is tested against multiple observables from cosmology, direct DM detection experiments and LHC searches. For this analysis we implemented the Lagrangian of the model in the LanHEP [42] and FeynRules [43] packages while model files have been generated in CalcHEP [44], FeynArts [45] and UFO [46] formats. The implementations have been cross-validated against each other and are available in the HEPMDB [47] repository. In addition, the LanHEP model files were cross-checked in both Unitary and t'Hooft-Feynman gauges within CalcHEP. We used micrOMEGAs v5.2.7 [48] for calculating DM observables and for setting the corresponding limits (see section IV A) as well as for the evaluation of some LHC processes. The model implementation in UFO format has been used in MG5_aMC [49] for the determination of the complete set of LHC constraints (see section IV B). The FeynArts model files from LanHEP were used to generated one-loop corrections to masses of $SU(2)_D$ gauge bosons by FeynCalc [50], FeynHelpers [51] and Package-X [52]. A simplified version of the model has been

implemented to calculate cross-sections at one-loop level in MG5_aMC and FormCalc9.8 [53].

A. Constraints from DM relic density, direct and ID

There are many non-collider experiments dedicatedly searching for signals of DM in space and on the Earth which play a very important role in limiting the DM parameter space and in the identification of viable DM models. These experiments are devoted to the precise determination of DM relic density as well as to Direct (DD) and Indirect Detection (ID) of DM. In particular, the PLANCK experiment has measured the relic density with a precision better than 1% [54]:

$$\Omega_{\rm DM}^{\rm Planck} h^2 = 0.12 \pm 0.0012\,. \tag{4.5}$$

In our analysis, we will select points that satisfy this constraint, bearing in mind that points which predict a relic density below PLANCK constraint could still be allowed if new sources of DM exist besides V_D.

For DM DD we use the limits from XENON1T [55]. The XENON1T experiment provides the most stringent upper limit (compared to LUX (2017) and Panda-X (2017), see Fig.5 in the reference [55]). Afterwards, we will refer to the DD limit as the one from XENON1T. The result from XENON1T is reported as DM-nucleon's cross-section as a function of DM mass with the range of $M_{DM} = [60, 1000]$ GeV. We have evaluated the DM spin-independent cross-section off proton by using the micrOMEGAs package. In order to compare micrOMEGAs' result with XENON1T limit, we rescale the cross-section by

$$\hat{\sigma}_{\rm SI} = \left(\frac{\Omega_{\rm DM}}{\Omega_{\rm DM}^{\rm Planck}}\right)\sigma_{\rm SI}, \tag{4.6}$$

and exclude points for which $\hat{\sigma}_{\rm SI}/\sigma_{\rm SI}^{\rm Xenon1T} > 1$.

ID DM searches are being performed by many experiments, including Fermi-LAT [56], IceCube [57], ANTARES [58], etc. However, these experiments rely on the DM local density and velocity distribution as well as the propagation of the particles in the galactic plane, and, therefore, the respective predictions are affected by various uncertainties of astronomical nature. To be independent of these uncertainties, in this study, we use the Cosmic Microwave Background (CMB) limit on DM ID based on PLANCK data. We consider the product of the DM-self annihilation or the DM decay into SM particles. By studying the effect of energy injection from DM annihilation products (electrons, positrons, gamma-ray, neutrinos and anti-protons) to the galactic medium which is sensitive to the CMB anisotropies, the upper limit on the energy injection measured by PLANCK is:

$$P_{\rm ann} < 3.2 \times 10^{-28}\ \frac{\rm cm^3}{\rm s\,GeV} \quad \text{at 95\% C.L.}, \tag{4.7}$$

with

$$P_{\rm ann} = \sum_j \frac{f_j^{\rm eff}\,\langle\sigma v\rangle_j}{M_{\rm DM}}\left(\frac{\Omega_{\rm DM}}{\Omega_{\rm DM}^{\rm Planck}}\right)^2, \tag{4.8}$$

where $\langle\sigma v\rangle_j$ is the thermally averaged partial annihilation cross-section for the j channel while $f_j^{\rm eff}$ is the energy fraction of DM annihilation transferring to the plasma for the jth channel. To construct the quantity $P_{\rm ann}$, we use micrOMEGAs to calculate $\langle\sigma v\rangle_j$ for all possible channels and neglect those that contribute to the total annihilation cross-section less than 0.1%. The effective fraction of energy $f_j^{\rm eff}$ was thoroughly studied and provided for almost all DM annihilation processes into two SM particles in the final state in [59, 60]. For non-SM particles in the final state of $2 \to 2$ processes, for example $V_D, V_D \to V', V'/V', H/H, H$, we make the approximation $f_{\text{non-SM}}^{\rm eff} \sim f_{q\bar{q}}^{\rm eff}$. This approximation is reasonable because each V_D/H eventually decays into 3 pairs of quarks anti-quarks and the energy fractions stored in each quark anti-quark pair (u, d, s, c, b, t) are not significantly different. The annihilation cross-section in eq. (4.8) is rescaled by $(\Omega_{\rm DM}/\Omega_{\rm DM}^{\rm Planck})^2$ due to the two DM particles in the initial state.

We have finally checked that the model does not spoil predictions from BBN when the life time of V' is too long, such that it decays during or after BBN, eventually spoiling the observed neutron to proton density ratio. For $m_{V'} \lesssim 2m_W$, the dominant decay to $b\bar{b}$ via the loop-induced process discussed above makes V' lifetime much shorter than the value excluded by BBN. So, in this respect, BBN does not exclude any region of the parameter space of our model that is allowed by relic density constraints.

B. Collider constraints

In the scenario under consideration the top quark is the only SM particle which interacts with the dark sector. Processes involving top quarks in propagators or final states are therefore affected by new physics contributions. The model contains a complex vector DM candidate but two different kind of mediators: the VL and $\mathbb{Z}_2$-odd top partner t_D and the two $\mathbb{Z}_2$-even bosons H and V', which however can only be produced at the LHC via interactions with the top quark or its $\mathbb{Z}_2$-even partner t'.

A list of relevant signatures for the scenario are provided in tab. III. A mono-jet signature can only arise at loop level, while the $t\bar{t}+E_T^{\rm miss}$ and $t\bar{t}t\bar{t}$ one can receive both tree- and loop-level contributions, which might be of similar size depending on the regions of parameter and phase space. Given the preliminary and explorative nature of this

Process	Representative diagrams
mono-jet (only loop)	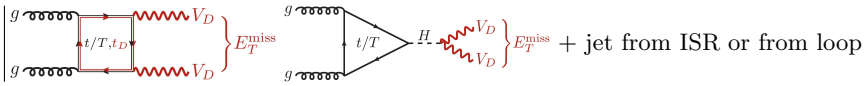 + jet from ISR or from loop
$t\bar{t}+E_T^{\rm miss}$	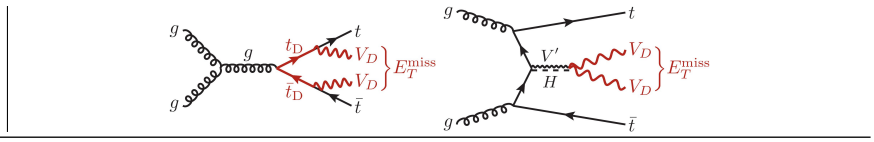
$t\bar{t}t\bar{t}$	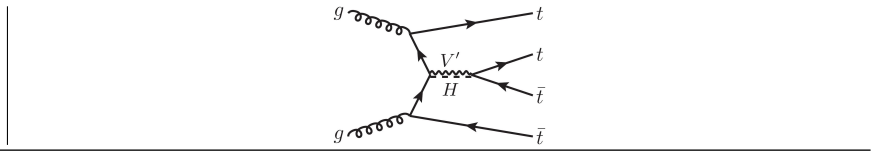
hV' and $V'V'$ (only loop)	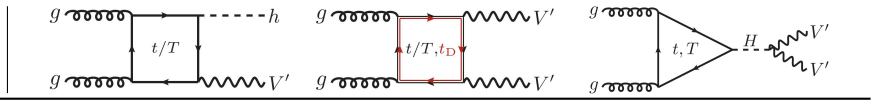

TABLE III. List of relevant processes at the LHC. $\mathbb{Z}_2$-odd particles are highlighted in red. Due to its purely VL nature, t_D cannot interact with the scalars.

analysis, in the following, we perform a recast of current LHC searches only for the tree-level processes to obtain constraints on the parameter space of the model.

The simulations are performed at Leading Order (LO) with MG5_aMC [49] in the 4-flavour scheme using the NNPDF3.0 LO set [61] through the LHAPDF 6 library [62] (LHA index 262400). No resonant propagation of new particles is imposed, to allow for the inclusion of interference and off-shellness effects when relevant. For the $t\bar{t}+E_T^{\rm miss}$ signature, in the region of a small mass gap between t_D and V_D, where $m_{t_D}-m_{V_D}<m_t$, simulations are performed for the $2\to 6$ process $pp\to W^+bW^-\bar{b}V_DV_D$. The recast is done through the MadAnalysis 5 framework and the searches considered for the recast are different depending on the process:

- for the $t\bar{t}+E_T^{\rm miss}$ processes we used a CMS search for top squark pair production decaying to DM, in final states with opposite sign leptons and missing transverse energy $E_T^{\rm miss}$ [63], recast in [64].

- for the $t\bar{t}t\bar{t}$ processes we used a CMS search for four top quarks in final states with either a pair of same-sign leptons or at least three leptons, in addition to multiple jets [65], recast in [66].

In both cases, the searches target the very same final states predicted by our model, and are therefore ideal for determining constraints from collider.

The loop-level diagrams can be relevant especially when the particles which decay to the final states are produced resonantly: in this case the loop suppression can be compensated by the lower multiplicity in the phase space. For the hV' and $V'V'$ processes we have only computed cross-sections using a simplified version of the model suitable for one-loop calculations in MG5_aMC, to estimate if they can be tested against data from current searches.

C. Combined bounds

We explore the viable parameter space of our model as well as the effect of the cosmological and collider constraints by performing a comprehensive scan over the 5D parameter space in the following ranges:

$$\begin{cases} 10^{-3} < g_D < 4\pi \\ 10 \text{ GeV} < m_{V_D} < m_{t_D} \\ m_t < m_{t_D} \leq m_T < 10^4 \text{ GeV} \\ 10 \text{ GeV} < m_H < 10^4 \text{ GeV} \end{cases} . \tag{4.9}$$

In fig. 5 we present the results of this scan showing projections into various planes: (m_{V_D}, g_D) (a), (m_H, m_{V_D}) (b), (m_{t_D}, m_{V_D}) (c) and (m_{t_D}, g_D) (d). The allowed parameter space is indicated by the green, cyan and blue regions,

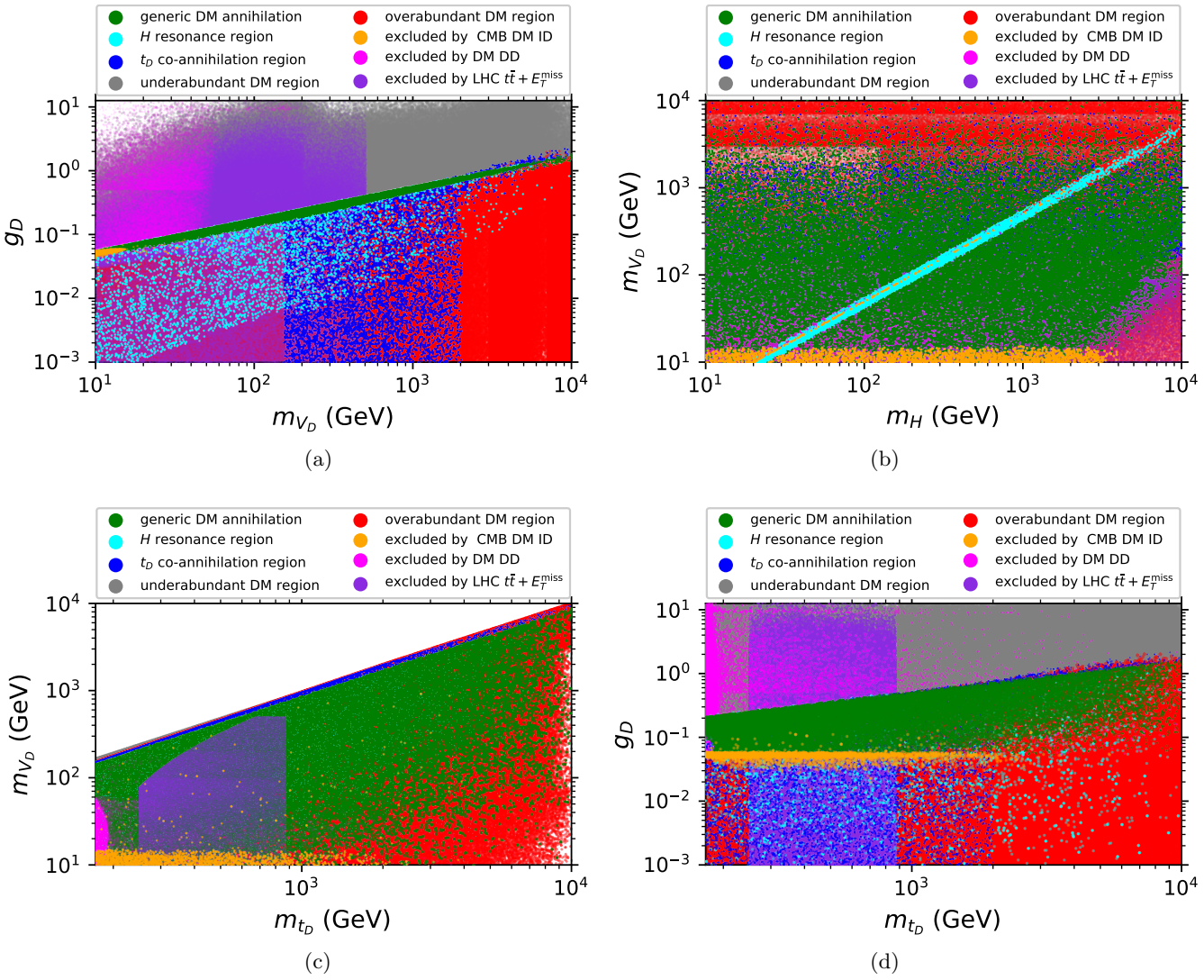

FIG. 5. Excluded and allowed region of the parameter space of the model from the full five-dimensional scan of the parameter space projected into (m_{V_D}, g_D), (m_H, m_{V_D}), (m_{t_D}, m_{V_D}) and (m_{t_D}, g_D) planes. The white areas represent: top-left corner of panel (a) – non-perturbative region of the parameter space; panel (b) – kinematically inaccessible $m_{V_D} > m_{t_D}$ region.

corresponding to generic DM annihilation (via $V_D V_D \to V'V'$ and t-channel $V_D V_D \to t\bar{t}$ processes), resonant (H) annihilation and DM$-t_D$ co-annihilation regions respectively. The representative Feynman diagrams for these channels are shown in fig. 6. In these regions the relic density constraint from PLANCK is satisfied within 5%. The grey colour indicates the under-abundant DM relic density region. From fig. 5(a) one can see that the generic DM annihilation (diagrams (a)–(c) of fig. 6) determines a narrow strip in the (g_D, m_{V_D}) plane indicating the correlation between g_D

and m_{V_D} to arrange the right amount of DM. For values of g_D below this band these processes cannot provide large enough cross-section for DM annihilation and this leads to the excluded over-abundant DM region indicated by the red colour. One can clearly see this region in all panels of fig. 5 for large DM masses. However, there are additional processes which provide an effective DM annihilation and respectively low DM relic density, consistent with PLANCK data. One of them is $V_D V_D \to H$ resonant annihilation, representative diagram for which is shown in fig. 6(d). This process allows one to extend the viable parameter space into the lower region of g_D (by up to two orders of magnitude) indicated by the cyan colour. This can be clearly seen in fig. 5(b), which presents the cyan H resonant band which goes across the whole parameter space in the (m_H, m_{V_D}) plane.

Another process, the DM-t_D co-annihilation channel (see representative diagram in fig. 6(e)), provides viable parameter space even for lower values of g_D for $m_{V_D} > m_t$ and m_{t_D} values below 2 TeV. The respective region is indicated by the blue colour, which can be clearly seen especially in (m_{t_D}, m_{V_D}) as a narrow resonance band. At the same time, when m_{V_D} is above 2 TeV, neither DM-t_D co-annihilation nor H-resonant annihilation are effective enough to provide low enough relic density for g_D values below the generic DM annihilation region. Therefore, the region with low g_D and large m_{V_D} is excluded due to the over-abundant relic density indicated by the red colour.

Furthermore, notice that the regions with low m_{V_D} and large g_D values are partly excluded by DD and/or ID experiments as indicated by magenta and orange points, respectively. The region of DM masses which can be tested and excluded by the LHC is presented by the violet region. This parameter space, which can be seen in all panels of fig. 5, is related to constraints on the $t\bar{t} + E_T^{\rm miss}$ signal at the LHC coming from $t_D \bar{t}_D$ pair production. For the masses of t_D below about 900 GeV this signal would be observed if there is enough phase space for $t_D \to V_D t$ decay. This process is important in setting one of the main collider constraints on the model under study.

The four projections presented in fig. 5 allow one to understand better and reveal the non-trivial shapes of the allowed and excluded regions over the 5D parameter space of the model. For example, the orange colour, which presents the DM ID exclusion region, takes place for $m_{V_D} < 20$ GeV (fig. 5(a,b,c)), $g_D \lesssim 0.06$ GeV (fig. 5(a,d)) and $m_H \lesssim 3$ TeV(fig. 5(b)). In Fig. fig. 5(b), one can see that DM ID exclusion takes place (besides the low m_{V_D} region discussed above) also along the very middle of the cyan band, where $m_{V_D} = m_H/2$. Indeed, in this case, DM effectively annihilates through the H state into $t\bar{t}$, $V'V'$ or gg, distorting precise CMB data, which therefore also limit the model parameter space. This region cannot be clearly seen in other panels, where it is presented just by randomly scattered points.

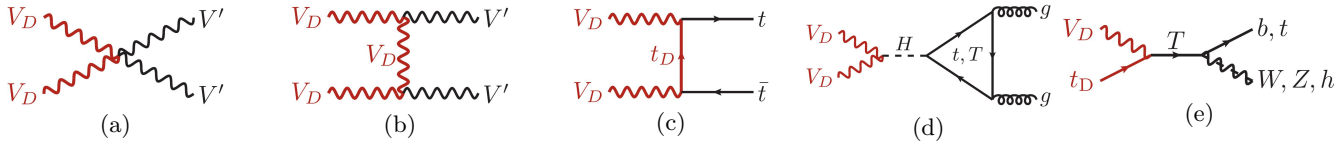

FIG. 6. Representative contributions to relic density. From left to right: 4-leg; t-channel DM annihilation; DM annihilation via resonant H; DM-mediator co-annihilation. $\mathbb{Z}_2$-odd particles are highlighted in red.

In order to assess the relative role of the different constraints in identifying the allowed region of parameter space of our model we identify different benchmarks, characterised by fixed values for the masses of the $\mathbb{Z}_2$-even top partner, $m_T = 1600$ GeV, and of the new scalar, $m_H = 1000$ GeV, as well as different values of the new gauge coupling $g_D = \{0.05, 0.1, 0.2, 0.5\}$. These choices have the following rationale: 1) the gauge coupling can either assume a small value for which constraints from over-abundant relic density only allow tiny regions of the parameter space or a larger value for which such constraints become weaker; 2) the $\mathbb{Z}_2$-even partner of the top is heavy enough to evade current LHC bounds based on pair production and considering decays into SM final states [41]; 3) the mass of the H state is large enough for it to decay into a top-quark pair. This affects the relative contribution of the diagrams mediated by H in table III.

The complementarity of cosmological and collider constraints can be represented in the $\{m_{t_D}, m_{V_D}\}$ or $\{m_{t_D}, 1 - \frac{m_{V_D}}{m_{t_D}}\}$ planes. The former, shown in fig. 7, allows us to highlight the low m_{V_D} region while the latter, shown in fig. 8, emphasises the small mass gap region between t_D and the DM particle. The interplay between relic density constraints and LHC bounds is largely sensitive to the gauge coupling value. For smaller values of the gauge coupling, $g_D = 0.05$ and $g_D = 0.1$, the measured amount of relic density is reconstructed only for light DM masses, $m_{V_D} \sim \mathcal{O}(10)$ GeV, and in a narrow region where the mass splitting between t_D and the DM is small, less than $\sim 10\%$ of m_{t_D}.

In the small m_{V_D} region, strong constraints from ID limit the allowed parameter space to m_{t_D} values approaching m_T, i.e. the region where the mixing between T and t becomes small. ID constraints however disappear for increasing values of g_D, corresponding to a reduction of relic density values, due to the scaling reported in eq. (4.8). Furthermore, the region with small m_{V_D} and either minimal or maximal mixing in the fermion sector is excluded by DD constraints. The weakness of such constraints are expected due to the suppressed interactions of the DM with the gluons in the nuclei, only possible at one-loop level via mediation of the top or its partners through the diagrams shown in fig. 9.

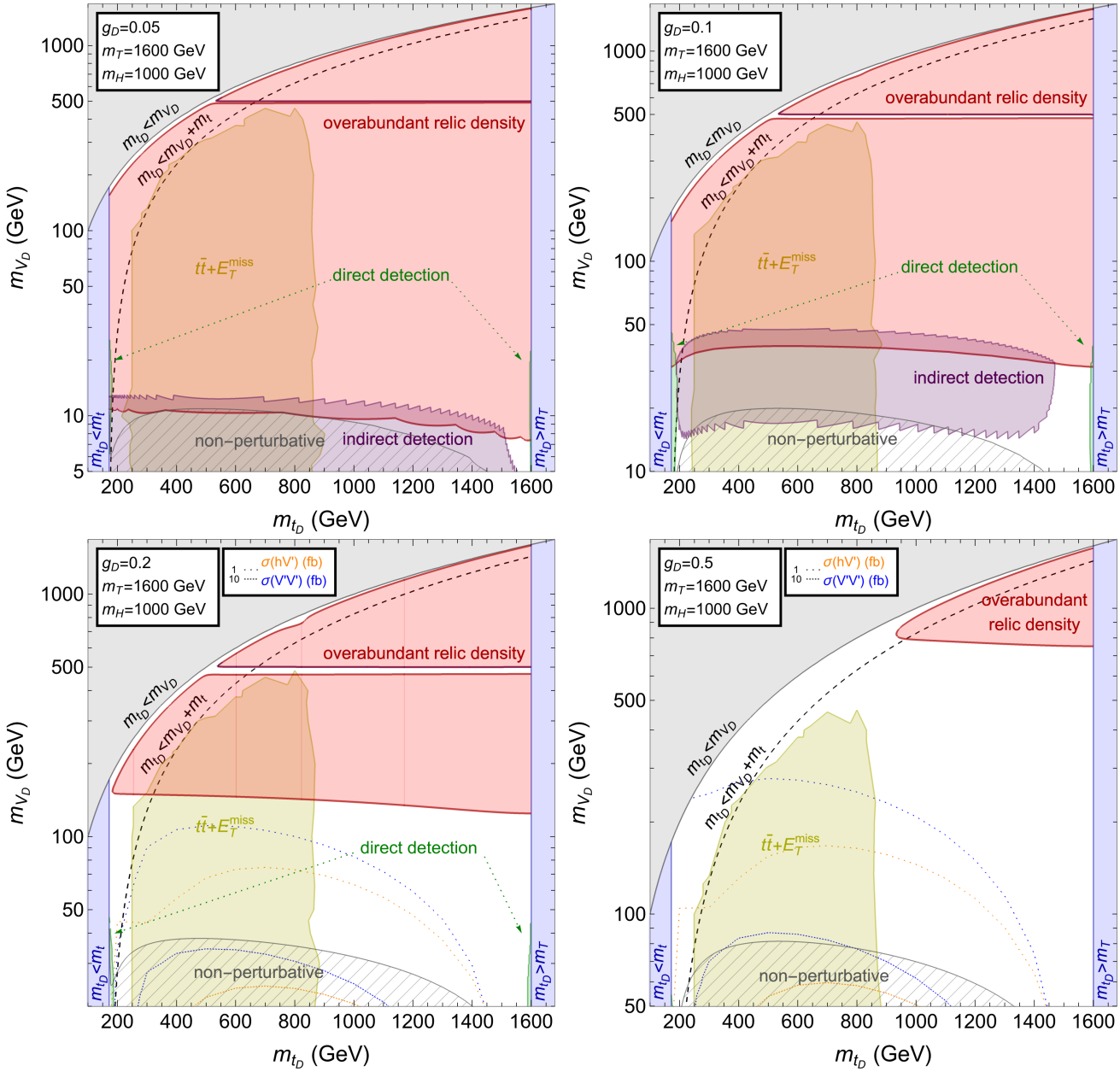

FIG. 7. Combination of constraints from LHC, relic density ID and DD in the $\{m_{t_D}, m_{V_D}\}$ plane for $m_T = 1600$ GeV, $m_H = 1000$ GeV and different values of g_D. The coloured regions are excluded. The measured relic density value is reconstructed on the borders of the excluded region. When constraints from ID are absent, cross-sections for hV' and $V'V'$ production processes are shown. The non perturbative region corresponds to corrections to the gauge boson masses larger than 50%.

Co-annihilation processes become effective in the region where the mass gap between V_D and t_D is tiny and in a narrow region centered around $m_{V_D} = m_H/2$, where H is produced resonantly and decays into gluons via top and T loops. In these areas the relic density is drastically reduced, becoming under-abundant. The small bell-shaped area visible in the middle of each panel of fig. 8 with $g_D < 0.5$ corresponds to the process in which T is produced resonantly and decays into SM final states Wb, Zt or ht, see fig. 6. If the gauge coupling becomes large enough, it becomes eventually impossible to reconstruct the measured value of the relic density and the entire allowed parameter space of the model corresponds to an under-abundant relic density. In this case, the theory would not be able to explain the whole observed DM content of the universe and other sources of DM would be needed.

The LHC bound comes exclusively from the $t\bar{t}+E_T^{\rm miss}$ signature, dominated by the pair production of t_D states. The bound is almost independent of the mass of t_D and constrains the region 250 GeV $\lesssim m_{t_D} \lesssim$ 850 GeV, independently of g_D, until the mass difference between t_D and the DM becomes small: in this case the missing energy component

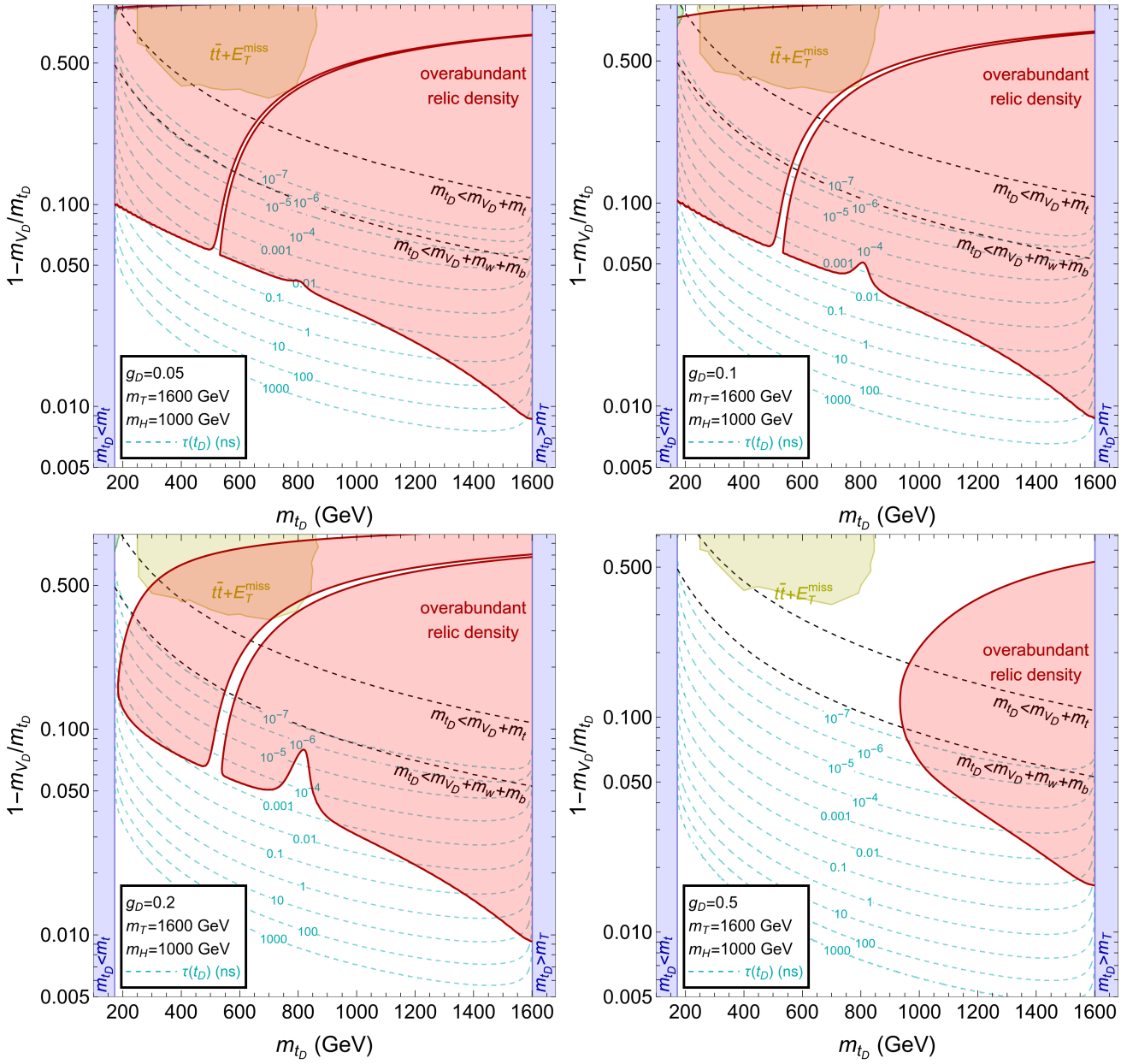

FIG. 8. Same as fig. 7 in the plane $\{m_{t_D}, 1-\frac{m_{V_D}}{m_{t_D}}\}$, to highlight the region where the DM and t_D have a small mass splitting. Contours corresponding to the lifetime of t_D (in a region where it can be long-lived) are also shown.

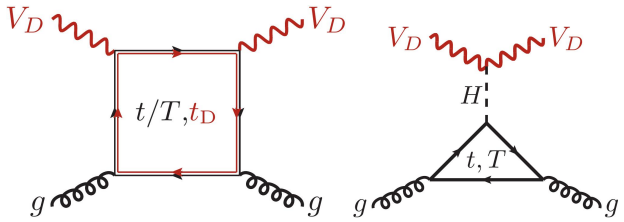

FIG. 9. Representative diagrams for direct detection processes. $\mathbb{Z}_2$-odd particles are highlighted in red.

of the events decreases and the sensitivity of the relevant CMS search reduces, allowing the small mass gap region. Effects coming from the width of t_D are negligible, as the t_D is narrow in the whole parameter space for each choice of g_D. The 4-top-quark search does not show any sensitivity over the whole parameter space, regardless of the value of

g_D. The loop processes of hV' associate production and $V'V'$ pair production are not testable at current luminosities, as their cross-sections are always well below $\sigma \gtrsim \mathcal{O}(10\text{ fb})$ in the region where relic density is reconstructed. Higher luminosities and/or higher energies would be needed to be sensitive to such final states.

A very interesting feature of this scenario emerges for small values of g_D in the small region where the DM and t_D have a small mass gap: the decay width of t_D becomes significantly small, such that t_D becomes long-lived (its lifetime in the small mass gap region is shown in fig. 7) and can be probed by dedicated searches at the LHC or future colliders. Different T or H masses would not modify this qualitative picture.

As a general conclusion, the combination of the relic density and LHC bounds always favours the region with large t_D mass if the mass difference with the DM is large, or any allowed value of m_{t_D} if the mass splitting between t_D and the DM is tiny. This specific realisation of the model is in any case an example dictated by its simple features. Including mixing in the scalar sector, further VL partners or further interactions of the same VL representation would enlarge the possible signatures and change the complementarity between different observables in constraining the model, potentially opening up further new interesting signatures.

V. CONCLUSIONS

To summarise, in this paper, we have defined a new class of FPVDM scenarios based on an additional $SU(2)_{\rm D}$ dark gauge group connected to the SM symmetry structure through a VL fermion mediator. As such, this scenario does not require a Higgs portal mediating the interactions between the dark sector and the standard one. A spontaneous breaking of the $SU(2)_{\rm D}$ symmetry provides the mass to the triplet of the respective gauge bosons. Two of these, which possess a $\mathbb{Z}_2$ symmetry, different from that of the SM, become DM candidates. This $\mathbb{Z}_2$ symmetry, providing stability to the DM state, can naturally be interpreted in the context of a dark EW sector or of the possible composite nature of the dark sector. Furthermore, such a model is renormalisable and therefore does not contain gauge kinetic mixing, although appropriate (mass) mixing in the gauge sector is normally present.

This general framework allows for multiple realisations, depending on the specific properties of the VL partner and the actual form of the scalar potential. As a simple example, herein, we have studied the case of a VL top-quark partner and no mixing between the SM Higgs doublet and the new scalar sector, which we have therefore called a 'top portal'. We have explored the phenomenology of such a minimal scenario and have provided bounds from both collider (chiefly, the LHC) and astroparticle (relic density, DD and ID) observables sensitive to the presence of DM, specifically discussing the role of the new states and interactions. In doing so, we have found that LHC and non-collider search experiments have significant complementary power to decode the scenario under study provided that several interesting signatures are observed. The signals could include direct or circumstantial evidence of the simultaneous presence of VL t_D and T quarks and/or the new H and/or V_D and V' bosons from $SU(2)_D$ in both open (i.e, real) and closed (i.e., virtual) production of such new physics states.

In fact, the specific BSM scenario introduced here presents one with the unique possibility of a multi-prong approach to a variety of distinctive signatures which would serve the purpose of enabling one to delineate all its key features. While we defer the detailed quantitative treatment of this approach to future publications, we highlight here what would be the salient features of it. The presence of a VL top companion T and its dark counterpart t_D subject to QCD interactions opens the obvious possibility of establishing their evidence at the LHC, through strong production processes. Furthermore, the additional Higgs and gauge states, as they couple to each other, would offer complementary evidence of such an extended dark sector, specifically, of its symmetry breaking pattern. Besides the generic mono-jet signature from V_D pair production (first row of diagrams in table III), which is hard to use to measure the model parameters, including the DM mass itself, there are several important complementary signals. Among these, there is associated production of V_D pairs with a $t\bar{t}$ one, yielding $t\bar{t}+E_T^{\rm miss}$, granting certain sensitivity to the presence of V' and H propagation. This can be achieved via the study of the momentum recoiling against the top-antitop system in the transverse plane (second graph in the second row of diagrams in table III). Indeed, the same final state may also make manifest the presence of the dark state t_D in a peculiar form, when it becomes a LLP exhibiting a displaced vertex, wherein a charged track (or invisible neutral dark hadron) would decay into the DM itself and SM hadrons and/or leptons. A measurement of the (proper) decay length of this signature could offer one the chance of extracting the value of the t_D width and use this information to decode related model parameters. Furthermore, the presence of V' and H states would be even clearer in $4t$ final states (diagram in the third row in table III), especially when the transitions $V' \to t\bar{t}$ and $H \to t\bar{t}$ are resonant. All such processes are potentially accessible at Run 3 of the LHC already. Furthermore, when the High Luminosity LHC (HL-LHC) option of the CERN machine will become available, also hV' and $V'V'$ production and decay would be accessible (fourth row of diagrams in table III). Finally, it is worth to mention that, if the V' mass is below the $t\bar{t}$ threshold, it can be long-lived and dominantly decay to $b\bar{b}$ pairs through loop-induced diagrams. In this case, hV' or $V'V'$ production would provide new striking signatures such as associate Higgs boson production together with a displaced $b\bar{b}$ resonance or pairs of $b\bar{b}$ displaced resonances,

respectively.

As a further outlook to our work, we would like to emphasise the following. The minimal realisation of a FPVDM scenario adopted here has already significant potential to explain astrophysical DM phenomena as well as to exhibit smoking gun signals at the LHC. However, non-minimal FPVDM models, which structure depends upon the concrete realisation of the mediator, Higgs and/or flavour sectors, would imply an even richer set of predictions and could well be used to explain currently observed data anomalies. For example, if the VL fermion interacts with the leptonic sector of the SM, it might explain lepton flavour anomalies at the LHC [67] or in $(g-2)_\mu$ [68] while at the same time provide novel physics cases for future e^+e^- colliders [69–72]. Finally, upon allowing for mixing in the scalar sector, further VL partners and/or additional interactions of the same VL representation, would open up a long list of possibilities for future studies, both theoretical and experimental. This would allow one to also explore the complementarity between collider and non-collider observables in such scenarios in ever greater depth than can be afforded by the minimal realisation tackled here.

ACKNOWLEDGEMENTS

AB and SM acknowledge support from the STFC Consolidated Grant ST/L000296/1 and are partially financed through the NExT Institute. AB also acknowledge support from Soton-FAPESP grant. LP's work is supported by the Knut and Alice Wallenberg foundation under the SHIFT project, grant KAW 2017.0100. AD is grateful to the LABEX Lyon Institute of Origins (ANR-10-LABX-0066) for its financial support within the program"Investissements d'Avenir". NT is supported by the scholarship from the Development and Promotion of Science and Technology Talents Project (DPST). All authors acknowledge the use of the IRIDIS High-Performance Computing Facility and associated support services at the University of Southampton in completing this work.

Appendix A: Mass splitting at one loop

At tree level, the neutral and charged components of $SU(2)_D$ gauge triplet are degenerate in mass as one can see in eq. (2.21). Nevertheless, the radiative correction at one-loop level breaks their mass degeneracy. The difference between m_{V_D} and $m_{V'}$ takes place due to the $T-t$ mixing and the different $\mathbb{Z}_2$ parities of the members of the $SU(2)_D$ fermion doublet, which results in distinct particles circling in the loops. In the limit $m_T \to m_{t_D}$ there is no mixing between the $T-t$ quarks, and the radiative corrections give zero contribution to masses of new vector bosons.

Loops involving the two scalars h and H are non-zero in case of mixing in the scalar sector. However, the contribution of such loops is identical for V_D and V' and therefore they will not be considered in the calculation of mass differences. We provide only fermion-loop diagrams in Unitary gauge, but we have cross-checked the results from both Unitary and Feynman-'t Hooft gauges to ensure that our results are gauge-independent.

In fig. 1 all possible self-energy diagrams with fermions circulating in the loops for V_D and V', contributing to a two-point function at one loop, are reported.

The self-energy amplitude of a vector boson can be decomposed into two components: the transverse and longitudinal ones.

$$i\Pi_V^{\mu\nu}(p^2) = \left(g^{\mu\nu} - \frac{p^\mu p^\nu}{p^2}\right) i\Pi_V^T(p^2) + \left(\frac{p^\mu p^\nu}{p^2}\right) i\Pi_V^L(p^2)\ , \tag{A1}$$

where Π_V^T and Π_V^L are the transverse and longitudinal amplitudes, respectively. Here we use a symbol V to indicate either V_D or V'.

We define the pole mass according to the position of the propagator's pole at one loop level, given by

$$m_V^{\text{pole}} = \sqrt{m_V^2 + \text{Re}(\Pi_V^T)}\ , \tag{A2}$$

where m_V is the tree-level mass, which is the same for both V_D and V', and we have suppressed the argument of the Π^T function. In order to find the physical mass splitting between V_D and V', we expand eq. (A2) in a power series.

$$m_V^{\text{pole}} = m_V \sum_{n=0}^{\infty} (-1)^n \binom{\frac{1}{2}}{n} \left(\frac{\text{Re}(\Pi_V^T)}{m_V^2}\right)^n\ , \tag{A3}$$

and truncate it at first order.

With the above argument, the pole mass splitting reads

$$\Delta m_V = m_{V_D}^{\rm pole} - m_{V'}^{\rm pole} = \frac{1}{2}\left(\frac{{\rm Re}(\Pi^T_{V_D}) - {\rm Re}(\Pi^T_{V'})}{m_V}\right) . \tag{A4}$$

The transverse Π^T function for fermion loops is given by:

$$\begin{aligned}\Pi_V^{T,\rm fermion} = \frac{1}{16\pi^2}\big[&(C_L^2+C_R^2)(A_0(M_1^2)+A_0(M_2^2))\\ &-\big((C_L^2+C_R^2)(p^2-M_1^2-M_2^2)+4C_LC_RM_1M_2\big)B_0(p^2,M_1^2,M_2^2)\\ &-4(C_L^2+C_R^2)B_1(p^2,M_1^2,M_2^2)\big] ,\end{aligned} \tag{A5}$$

where the C_L and C_R is the left-projected and right-projected couplings of FFV vertices, respectively. The A_0, B_0 and B_1 are Passarino-Veltman scalar functions defined by

$$A_0(m) = m^2 + m^2\log\frac{\mu^2}{m^2} + \frac{m^2}{\epsilon} \tag{A6}$$

$$B_0(p^2,m_1^2,m_2^2) = 2 + f(p^2,m_1^2,m_2^2) - \frac{p^2+m_1^2-m_2^2}{2p^2}\log\frac{m_1^2}{m_2^2} + \log\frac{\mu^2}{m_2^2} + \frac{1}{\epsilon} \tag{A7}$$

$$\begin{aligned}B_1(p^2,m_1^2,m_2^2) = &-\frac{f(p^2,m_1^2,m_2^2)\left((m_1^2-m_2^2)^2+p^2(p^2-2m_1^2-2m_2^2)\right)}{12p^2}\\ &-\frac{\left(3(m_1^2-m_2^2)^2+8p^4-21m_1^2p^2-21m_2^2p^2\right)}{36p^2}\\ &+\frac{\left((m_1^2-m_2^2)^3-3(m_1^4-m_2^4)p^2-3(m_1^2-m_2^2)p^4+p^6\right)}{24p^4}\log\frac{m_1^2}{m_2^2}\\ &+\frac{1}{12}(3m_1^2+3m_2^2-p^2)\left(\frac{1}{\epsilon}+\log\frac{\mu^2}{m_2^2}\right) ,\end{aligned} \tag{A8}$$

where

$$\begin{aligned}f(p^2,m_1^2,m_2^2) &= \frac{\sqrt{\lambda(m_1^2,m_2^2,p^2)}}{p^2}\log\left[\frac{m_1^2+m_2^2-p^2+\sqrt{\lambda(m_1^2,m_2^2,p^2)}}{2m_1m_2}\right],\\ \lambda(m_1^2,m_2^2,p^2) &= (m_1^2-m_2^2)^2-2(m_1^2+m_2^2)p^2+p^4 .\end{aligned} \tag{A9}$$

Here we use the modified minimal subtraction $\overline{\rm MS}$ renormalisation scheme, μ is the renormalisation scale and $\frac{1}{\epsilon}\to\frac{1}{\epsilon}-\gamma_E+\log 4\pi$. The fermion parts of Π functions (where the T superscript will now be suppressed for simplicity) are given by

$$\Pi_{V_D}^{\rm fermion} = \Pi_{V_D}^{t_D,t} + \Pi_{V_D}^{t_D,T} , \tag{A10}$$

$$\Pi_{V'}^{\rm fermion} = \Pi_{V'}^{t,t} + \Pi_{V'}^{t_D,t_D} + \Pi_{V'}^{t,T} + \Pi_{V'}^{T,T} , \tag{A11}$$

where

$$\begin{aligned}&C_L^{t_D,t} = -\frac{g_D}{\sqrt{2}}\sin\theta_{fL}, \quad C_R^{t_D,t} = -\frac{g_D}{\sqrt{2}}\sin\theta_{fR}, \quad C_L^{t_D,T} = \frac{g_D}{\sqrt{2}}\cos\theta_{fL}, \quad C_R^{t_D,T} = \frac{g_D}{\sqrt{2}}\cos\theta_{fR}\\ &C_L^{t,t} = -\frac{g_D}{2}\sin^2\theta_{fL}, \quad C_R^{t,t} = -\frac{g_D}{2}\sin^2\theta_{fR}, \quad C_L^{t_D,t_D} = C_R^{t_D,t_D} = \frac{g_D}{2},\\ &C_L^{t,T} = \frac{g_D}{2}\sin\theta_{fL}\cos\theta_{fL}, \quad C_R^{t,T} = \frac{g_D}{2}\sin\theta_{fR}\cos\theta_{fR}, \quad C_L^{T,T} = -\frac{g_D}{2}\cos^2\theta_{fL}, \quad C_R^{T,T} = -\frac{g_D}{2}\cos^2\theta_{fR} .\end{aligned} \tag{A12}$$

We can find a very simple and elegant formula for mass splitting by substituting eqs. (A5), (A10) and (A12) into eq. (A4), and then writing the result in terms of

$$\epsilon = \frac{m_T^2-m_{t_D}^2}{m_T^2}, \quad \epsilon_2 = \frac{m_t^2}{m_T^2}, \quad \epsilon_3 = \frac{m_V^2}{m_T^2} . \tag{A13}$$

In the approximation that $\epsilon, \epsilon_2, \epsilon_3 \ll 1$, the mass splitting reads

$$\Delta m_V' = \frac{1}{640\pi^2 m_{V_D}}\epsilon g_D^2 m_T^2\left[(20+3\epsilon_3-15\epsilon_2+20\epsilon_2\epsilon_3)+10(2\epsilon_2-\epsilon_3-2\epsilon_2\epsilon_3)\log\epsilon_3\right] . \tag{A14}$$

It is possible to simplify the above result further by keeping only the leading term of ϵ as

$$\Delta m_V'' = \frac{g_D^2 m_T^2}{32\pi^2 m_{V_D}} \frac{m_T^2 - m_{t_D}^2}{m_T^2} \ . \tag{A15}$$

Appendix B: Mixing structure in the gauge sector for the dark EW sector

Defining $\mathcal{V}^0_{D0\mu} = (B_\mu, W^3_\mu, B^0_{D0\mu}, V^0_{D0\mu})^T$ and using analogous notation as eq.(2.20) for the fully neutral gauge boson Lagrangian term after EW and dark symmetry breaking,

$$\mathcal{L}^{\rm kin}_{\mathcal{V}^0_{D0}}|_{v,v_D} \supset (\mathcal{V}^0_{D0})^T \mathcal{M}^2_{\mathcal{V}^0_{D0}} \mathcal{V}^0_{D0} \ , \tag{B1}$$

the entries of the mass mixing matrix in the gauge sector are:

$$\mathcal{M}^2_{\mathcal{V}^0_{D0}}|_{11} = \frac{\left(g'^2 v^2 + g_D'^2 v_D^2 \epsilon^2\right)\cos^2\theta_k - g_D'^2 \epsilon\sqrt{1-\epsilon^2}\sin 2\theta_k v_D^2 + g_D'^2\left(1-\epsilon^2\right)\sin^2\theta_k v_D^2}{8\left(1-\epsilon^2\right)} \tag{B2}$$

$$\mathcal{M}^2_{\mathcal{V}^0_{D0}}|_{12} = \mathcal{M}^2_{\mathcal{V}^0_{D0}}|_{21} = -\frac{g g' v^2 \cos\theta_k}{8\sqrt{1-\epsilon^2}} \tag{B3}$$

$$\mathcal{M}^2_{\mathcal{V}^0_{D0}}|_{13} = \mathcal{M}^2_{\mathcal{V}^0_{D0}}|_{31} = \frac{g_D'^2 v_D^2\left(\left(1-2\epsilon^2\right)\sin 2\theta_k - 2\epsilon\sqrt{1-\epsilon^2}\cos 2\theta_k\right) - g'^2 \sin 2\theta_k v^2}{16\left(1-\epsilon^2\right)} \tag{B4}$$

$$\mathcal{M}^2_{\mathcal{V}^0_{D0}}|_{14} = \mathcal{M}^2_{\mathcal{V}^0_{D0}}|_{41} = \frac{1}{8} g_D g_D' v_D^2 \left(\frac{\epsilon\cos\theta_k}{\sqrt{1-\epsilon^2}} - \sin\theta_k\right) \tag{B5}$$

$$\mathcal{M}^2_{\mathcal{V}^0_{D0}}|_{22} = \frac{g^2 v^2}{8} \tag{B6}$$

$$\mathcal{M}^2_{\mathcal{V}^0_{D0}}|_{23} = \mathcal{M}^2_{\mathcal{V}^0_{D0}}|_{32} = \frac{g g' v^2 \sin\theta_k}{8\sqrt{1-\epsilon^2}} \tag{B7}$$

$$\mathcal{M}^2_{\mathcal{V}^0_{D0}}|_{24} = \mathcal{M}^2_{\mathcal{V}^0_{D0}}|_{42} = 0 \tag{B8}$$

$$\mathcal{M}^2_{\mathcal{V}^0_{D0}}|_{33} = \frac{g_D'^2\left(1-\epsilon^2\right)\cos^2\theta_k v_D^2 + g_D'^2 \epsilon\sqrt{1-\epsilon^2}\sin 2\theta_k v_D^2 + \left(g'^2 v^2 + g_D'^2 v_D^2 \epsilon^2\right)\sin^2\theta_k}{8\left(1-\epsilon^2\right)} \tag{B9}$$

$$\mathcal{M}^2_{\mathcal{V}^0_{D0}}|_{34} = \mathcal{M}^2_{\mathcal{V}^0_{D0}}|_{43} = -\frac{1}{8} g_D g_D' v_D^2 \left(\cos\theta_k + \frac{\epsilon\sin\theta_k}{\sqrt{1-\epsilon^2}}\right) \tag{B10}$$

$$\mathcal{M}^2_{\mathcal{V}^0_{D0}}|_{44} = \frac{g_D^2 v_D^2}{8} \ . \tag{B11}$$

The mass eigenstates corresponding to the eigenvalues of the mixing matrix are γ, γ_D, Z and Z'. Their masses do not depend on the rotation angle θ_k and read:

$$m_\gamma = m_{\gamma_D} = 0 \tag{B12}$$

$$M^2_{Z,Z'} = \frac{1}{8}\left[g^2 v^2 + g_D^2 v_D^2 + \frac{1}{1-\epsilon^2}\left(g'^2 v^2 + g_D'^2 v_D^2 \mp \sqrt{\mathcal{K}_0 + \mathcal{K}_2 \epsilon^2 + \mathcal{K}_4 \epsilon^4}\right)\right] \tag{B13}$$

where the $\mathcal{K}$ functions are defined as:

$$\mathcal{K}_0 = \left(\left(g^2 + g'^2\right) v^2 - \left(g_D'^2 + g_D^2\right) v_D^2\right)^2 \tag{B14}$$

$$\mathcal{K}_2 = -2\left[g^2(g^2+g'^2)v^4 + g_D^2(g_D^2 + g_D'^2)v_D^4 - \left(g^2(2g_D^2 + g_D'^2) + g'^2\left(g_D^2 + 2g_D'^2\right)\right) v^2 v_D^2\right] \tag{B15}$$

$$\mathcal{K}_4 = (g^2 v^2 - g_D^2 v_D^2)^2 \tag{B16}$$

and the sign in front of the square root is chosen to reconstruct the SM value of the Z mass for $\epsilon \to 0$ and $\left(g^2 + g'^2\right) v^2 > \left(g_D'^2 + g_D^2\right) v_D^2$.

[1] J. Hubisz and P. Meade, Phys. Rev. D **71**, 035016 (2005), arXiv:hep-ph/0411264.

[2] T. Hambye, JHEP **01**, 028 (2009), arXiv:0811.0172 [hep-ph].
[3] F. Chen, J. M. Cline, and A. R. Frey, Phys. Rev. D **80**, 083516 (2009), arXiv:0907.4746 [hep-ph].
[4] J. Diaz-Cruz and E. Ma, Phys. Lett. B **695**, 264 (2011), arXiv:1007.2631 [hep-ph].
[5] S. Bhattacharya, J. Diaz-Cruz, E. Ma, and D. Wegman, Phys. Rev. D **85**, 055008 (2012), arXiv:1107.2093 [hep-ph].
[6] O. Lebedev, H. M. Lee, and Y. Mambrini, Phys. Lett. B **707**, 570 (2012), arXiv:1111.4482 [hep-ph].
[7] Y. Farzan and A. R. Akbarieh, JCAP **10**, 026 (2012), arXiv:1207.4272 [hep-ph].
[8] E. Koorambas, Int. J. Theor. Phys. **52**, 4374 (2013).
[9] S. Fraser, E. Ma, and M. Zakeri, Int. J. Mod. Phys. A **30**, 1550018 (2015), arXiv:1409.1162 [hep-ph].
[10] P. Ko, W.-I. Park, and Y. Tang, JCAP **09**, 013 (2014), arXiv:1404.5257 [hep-ph].
[11] W.-C. Huang, Y.-L. S. Tsai, and T.-C. Yuan, JHEP **04**, 019 (2016), arXiv:1512.00229 [hep-ph].
[12] C. Gross, O. Lebedev, and Y. Mambrini, JHEP **08**, 158 (2015), arXiv:1505.07480 [hep-ph].
[13] A. DiFranzo, P. J. Fox, and T. M. P. Tait, JHEP **04**, 135 (2016), arXiv:1512.06853 [hep-ph].
[14] P. Ko and Y. Tang, Phys. Lett. B **768**, 12 (2017), arXiv:1609.02307 [hep-ph].
[15] B. Barman, S. Bhattacharya, S. K. Patra, and J. Chakrabortty, JCAP **12**, 021 (2017), arXiv:1704.04945 [hep-ph].
[16] W.-C. Huang, H. Ishida, C.-T. Lu, Y.-L. S. Tsai, and T.-C. Yuan, Eur. Phys. J. C **78**, 613 (2018), arXiv:1708.02355 [hep-ph].
[17] B. Barman, S. Bhattacharya, and M. Zakeri, JCAP **09**, 023 (2018), arXiv:1806.01129 [hep-ph].
[18] B. Barman, S. Bhattacharya, and M. Zakeri, JCAP **02**, 029 (2020), arXiv:1905.07236 [hep-ph].
[19] D. Buttazzo, L. Di Luzio, P. Ghorbani, C. Gross, G. Landini, A. Strumia, D. Teresi, and J.-W. Wang, JHEP **01**, 130 (2020), arXiv:1911.04502 [hep-ph].
[20] T. Abe, M. Fujiwara, J. Hisano, and K. Matsushita, JHEP **07**, 136 (2020), arXiv:2004.00884 [hep-ph].
[21] C. Gross, S. Karamitsos, G. Landini, and A. Strumia, JHEP **03**, 174 (2021), arXiv:2012.12087 [hep-ph].
[22] T. A. Chowdhury and S. Saad, JCAP **10**, 014 (2021), arXiv:2107.11863 [hep-ph].
[23] N. Baouche, A. Ahriche, G. Faisel, and S. Nasri, Phys. Rev. D **104**, 075022 (2021), arXiv:2105.14387 [hep-ph].
[24] Z. Hu, C. Cai, Y.-L. Tang, Z.-H. Yu, and H.-H. Zhang, JHEP **07**, 089 (2021), arXiv:2103.00220 [hep-ph].
[25] S. Baek, P. Ko, and P. Wu, JCAP **07**, 008 (2018), arXiv:1709.00697 [hep-ph].
[26] S. Colucci, B. Fuks, F. Giacchino, L. Lopez Honorez, M. H. G. Tytgat, and J. Vandecasteele, Phys. Rev. D **98**, 035002 (2018), arXiv:1804.05068 [hep-ph].
[27] J. B. Jiménez, D. Bettoni, and P. Brax, Phys. Rev. D **103**, 103505 (2021), arXiv:2004.13677 [astro-ph.CO].
[28] G. Servant and T. M. P. Tait, Nucl. Phys. B **650**, 391 (2003), arXiv:hep-ph/0206071.
[29] G. Cacciapaglia, A. Deandrea, and J. Llodra-Perez, JHEP **03**, 083 (2010), arXiv:0907.4993 [hep-ph].
[30] F. Giacchino, A. Ibarra, L. Lopez Honorez, M. H. G. Tytgat, and S. Wild, JCAP **02**, 002 (2016), arXiv:1511.04452 [hep-ph].
[31] M. Garny, J. Heisig, M. Hufnagel, and B. Lülf, Phys. Rev. D **97**, 075002 (2018), arXiv:1802.00814 [hep-ph].
[32] C. Arina, B. Fuks, and L. Mantani, Eur. Phys. J. C **80**, 409 (2020), arXiv:2001.05024 [hep-ph].
[33] C. Arina, B. Fuks, L. Mantani, H. Mies, L. Panizzi, and J. Salko, Phys. Lett. B **813**, 136038 (2021), arXiv:2010.07559 [hep-ph].
[34] A. Belyaev, A. Deandrea, S. Moretti, L. Panizzi, and N. Thongyoi, (2022), arXiv:2203.04681 [hep-ph].
[35] M. Buchkremer, G. Cacciapaglia, A. Deandrea, and L. Panizzi, Nucl. Phys. B **876**, 376 (2013), arXiv:1305.4172 [hep-ph].
[36] G. Cacciapaglia, A. Deandrea, L. Panizzi, N. Gaur, D. Harada, and Y. Okada, JHEP **03**, 070 (2012), arXiv:1108.6329 [hep-ph].
[37] Y. Okada and L. Panizzi, Adv. High Energy Phys. **2013**, 364936 (2013), arXiv:1207.5607 [hep-ph].
[38] T. Ma and G. Cacciapaglia, JHEP **03**, 211 (2016), arXiv:1508.07014 [hep-ph].
[39] Y. Wu, T. Ma, B. Zhang, and G. Cacciapaglia, JHEP **11**, 058 (2017), arXiv:1703.06903 [hep-ph].
[40] D. Feldman, Z. Liu, and P. Nath, Phys. Rev. D **75**, 115001 (2007), arXiv:hep-ph/0702123.
[41] M. Aaboud *et al.* (ATLAS), Phys. Rev. Lett. **121**, 211801 (2018), arXiv:1808.02343 [hep-ex].
[42] A. Semenov, Computer Physics Communications **180**, 431–454 (2009).
[43] A. Alloul, N. D. Christensen, C. Degrande, C. Duhr, and B. Fuks, Comput. Phys. Commun. **185**, 2250 (2014), arXiv:1310.1921 [hep-ph].
[44] A. Belyaev, N. D. Christensen, and A. Pukhov, Comput. Phys. Commun. **184**, 1729 (2013), arXiv:1207.6082 [hep-ph].
[45] T. Hahn, Comput. Phys. Commun. **140**, 418 (2001), arXiv:hep-ph/0012260.
[46] C. Degrande, C. Duhr, B. Fuks, D. Grellscheid, O. Mattelaer, and T. Reiter, Comput. Phys. Commun. **183**, 1201 (2012), arXiv:1108.2040 [hep-ph].
[47] M. Bondarenko, A. Belyaev, J. Blandford, L. Basso, E. Boos, V. Bunichev, *et al.*, (2012), arXiv:1203.1488 [hep-ph].
[48] G. Belanger, A. Mjallal, and A. Pukhov, Eur. Phys. J. C **81**, 239 (2021), arXiv:2003.08621 [hep-ph].
[49] J. Alwall, R. Frederix, S. Frixione, V. Hirschi, F. Maltoni, O. Mattelaer, H. S. Shao, T. Stelzer, P. Torrielli, and M. Zaro, JHEP **07**, 079 (2014), arXiv:1405.0301 [hep-ph].
[50] V. Shtabovenko, R. Mertig, and F. Orellana, Comput. Phys. Commun. **256**, 107478 (2020), arXiv:2001.04407 [hep-ph].
[51] V. Shtabovenko, Comput. Phys. Commun. **218**, 48 (2017), arXiv:1611.06793 [physics.comp-ph].
[52] H. H. Patel, Comput. Phys. Commun. **218**, 66 (2017), arXiv:1612.00009 [hep-ph].
[53] T. Hahn, S. Paßehr, and C. Schappacher, PoS **LL2016**, 068 (2016), arXiv:1604.04611 [hep-ph].
[54] N. Aghanim *et al.* (Planck), Astron. Astrophys. **641**, A6 (2020), [Erratum: Astron.Astrophys. 652, C4 (2021)], arXiv:1807.06209 [astro-ph.CO].
[55] E. Aprile *et al.* (XENON), Phys. Rev. Lett. **121**, 111302 (2018), arXiv:1805.12562 [astro-ph.CO].

[56] M. Ackermann *et al.* (Fermi-LAT), Astrophys. J. **840**, 43 (2017), arXiv:1704.03910 [astro-ph.HE].
[57] M. G. Aartsen *et al.* (IceCube), JINST **12**, P03012 (2017), arXiv:1612.05093 [astro-ph.IM].
[58] A. Albert *et al.* (ANTARES, IceCube), Phys. Rev. D **102**, 082002 (2020), arXiv:2003.06614 [astro-ph.HE].
[59] T. R. Slatyer, Phys. Rev. D **93**, 023527 (2016), arXiv:1506.03811 [hep-ph].
[60] R. K. Leane, T. R. Slatyer, J. F. Beacom, and K. C. Y. Ng, Phys. Rev. D **98**, 023016 (2018), arXiv:1805.10305 [hep-ph].
[61] R. D. Ball *et al.* (NNPDF), JHEP **04**, 040 (2015), arXiv:1410.8849 [hep-ph].
[62] A. Buckley, J. Ferrando, S. Lloyd, K. Nordström, B. Page, M. Rüfenacht, M. Schönherr, and G. Watt, Eur. Phys. J. C **75**, 132 (2015), arXiv:1412.7420 [hep-ph].
[63] A. M. Sirunyan *et al.* (CMS), Phys. Rev. D **97**, 032009 (2018), arXiv:1711.00752 [hep-ex].
[64] S. Bein, S.-M. Choi, B. Fuks, S. Jeong, D. W. Kang, J. Li, and J. Sonneveld, "Implementation of a search for stops in the di-lepton + missing energy channel (35.9 fb-1; 13 TeV; CMS-SUS-17-001)," (2021).
[65] A. M. Sirunyan *et al.* (CMS), Eur. Phys. J. C **80**, 75 (2020), arXiv:1908.06463 [hep-ex].
[66] L. Darmé and B. Fuks, "Re-implementation of a search for four-top quark production with leptonic final states (137 fb-1; CMS-TOP-18-003)," (2020).
[67] A. Crivellin and M. Hoferichter, Science **374**, 1051 (2021), arXiv:2111.12739 [hep-ph].
[68] B. Abi *et al.* (Muon g-2), Phys. Rev. Lett. **126**, 141801 (2021), arXiv:2104.03281 [hep-ex].
[69] M. Aicheler, P. Burrows, M. Draper, T. Garvey, P. Lebrun, K. Peach, N. Phinney, H. Schmickler, D. Schulte, and N. Toge, (2012), 10.5170/CERN-2012-007.
[70] H. Baer *et al.*, (2013), arXiv:1306.6352 [hep-ph].
[71] F. An *et al.*, Chin. Phys. C **43**, 043002 (2019), arXiv:1810.09037 [hep-ex].
[72] A. Abada *et al.* (FCC), Eur. Phys. J. ST **228**, 261 (2019).